Commissureless acts as a substrate adapter in a conserved Nedd4 E3 ubiquitin ligase pathway to promote axon growth across the midline

Kelly G. Sullivan[1] and Greg J. Bashaw[1]*

[1]Department of Neuroscience, Perelman School of Medicine, University of Pennsylvania, 415 Curie Blvd., Philadelphia, PA, 19104, USA

* Author for correspondence: gbashaw@pennmedicine.upenn.edu

Running title: Nedd4 guides commissural axons

Keywords: Axon guidance; midline; Slit-Robo; Commissureless; Nedd4; E3 Ubiquitin ligase; lysosomal degradation; Ndfip

SUMMARY

In both vertebrates and invertebrates, commissural neurons prevent premature responsiveness to the midline repellant Slit by downregulating surface levels of its receptor Roundabout1 (Robo1). In *Drosophila*, Commissureless (Comm) plays a critical role in this process; however, there is conflicting data on the underlying molecular mechanism. Here, we demonstrate that the conserved PY motifs in the cytoplasmic domain of Comm are required allow the ubiquitination and lysosomal degradation of Robo1. Disruption of these motifs prevents Comm from localizing to Lamp1 positive late endosomes and to promote axon growth across the midline *in vivo*. In addition, we conclusively demonstrate a role for Nedd4 in midline crossing. Genetic analysis shows that *nedd4* mutations result in midline crossing defects in the Drosophila embryonic nerve cord, which can be rescued by introduction of exogenous Nedd4. Biochemical evidence shows that Nedd4 incorporates into a three-member complex with Comm and Robo in a PY motif-dependent manner. Finally, we present genetic evidence that Nedd4 acts with Comm in the embryonic nerve cord to downregulate Robo1 levels. Taken together, these findings demonstrate that Comm promotes midline crossing in the nerve cord by facilitating Robo ubiquitination by Nedd4, ultimately leading to its degradation.

INTRODUCTION

In the embryo, neurons must find and form connections with the appropriate synaptic partners as they wire circuits in the developing nervous system. To make these connections, axons must travel long distances along complex but stereotyped trajectories, directed by a variety of secreted and cell-surface molecules that are conserved from invertebrates to humans. Interaction between these ligands and receptors on the membranes of axonal growth cones generates attractive and repulsive responses by triggering downstream changes in growth cone membrane and cytoskeletal architecture. Responses to these attractive and repulsive cues must be precisely coordinated to allow axons to grow along the appropriate paths and to find their proper post-synaptic targets.

Bilateral organisms must form neural circuits that coordinate the left and right halves of the body, a process that is essential for normal sensory, motor, and cognitive function. Defects in midline circuit assembly can result in a variety of neurodevelopmental disorders (for reviews see (Engle, 2010; Izzi and Charron, 2011)) including horizontal gaze palsy with progressive scoliosis (Bosley et al., 2005), congenital mirror movement disorder (Depienne et al., 2011; Srour et al., 2010), autism spectrum disorder (Anitha et al., 2008; Suda et al., 2011), and agenesis of the corpus callosum (Jamuar et al., 2017; Paul et al., 2007). A subset of neurons in the central nervous system (CNS), called commissural neurons, contribute to the construction of these circuits by extending their axons across the embryonic midline to connect with targets on the opposite side of the body. Midline crossing requires a tight balance of attractive and repulsive responses (Evans and Bashaw, 2010; Gorla and Bashaw, 2020; Nawabi and Castellani, 2011). Pre-crossing commissural axons are initially drawn to the midline by several attractive ligands including netrin (Ishii et al., 1992; Mitchell et al., 1996; Serafini et al., 1996; Serafini et al., 1994) and sonic hedgehog (Charron et al., 2003). Upon reaching the midline, however, they respond to repulsive molecules such as slits and secreted semaphorins (Brose et al., 1999; Kidd et al., 1999; Zou et al., 2000) which allow them to exit the midline and keep them

64 restricted to the contralateral side of the body by preventing re-crossing. Midline glia secrete
65 both attractive and repulsive molecules concurrently, so an axon's behavior during a particular
66 moment in time relies on tight regulation of receptors at its growth cone surface.

67 Pre-crossing commissural axons must suppress premature responses to repulsive
68 signals to allow entry into the midline. In both vertebrates and invertebrates, axons prevent
69 premature sensitivity to the midline repellant Slit by downregulating surface levels of its
70 receptor, Robo1, until they reach the midline (Evans et al., 2015; Keleman et al., 2002;
71 Kinoshita-Kawada et al., 2019; Sabatier et al., 2004). In *Drosophila*, Robo1 surface expression
72 is downregulated by the Commissureless (Comm) protein (Keleman et al., 2002; Kidd et al.,
73 1998; Tear et al., 1996), which is absolutely required for midline crossing. Nerve cords of Comm
74 mutant embryos exhibit a complete lack of midline crossing (Tear et al., 1996), while Comm
75 overexpression decreases Robo1 levels and induces ectopic midline crossing events (Kidd et
76 al., 1998). Based on experiments in mammalian and insect cell culture, Comm is thought to act
77 by preventing newly synthesized Robo1 from reaching the growth cone membrane by binding to
78 it and shunting it to late endosomes, presumably leading to its degradation (Keleman et al.,
79 2002; Keleman et al., 2005).

80 While it is generally accepted that Comm prevents Robo1 from being expressed on the
81 growth cone in pre-crossing commissural axons, there are conflicting reports of the mechanism
82 of Comm function. Within a conserved region of the Comm cytoplasmic domain, there are two
83 PY motifs (PPCY and LPSY) (Myat et al., 2002). In a previous study, mutation of the LPSY motif
84 rendered Comm unable to localize Robo1 to endosomes in cell culture, and unable to induce
85 midline crossing *in vivo* (Keleman et al., 2002). PY motifs are known binding motifs for the WW-
86 domain containing Nedd4 family of HECT ubiquitin ligases (Kanelis et al., 2001; Kasanov et al.,
87 2001), suggesting that Comm may downregulate Robo1 via interactions with these ligases.
88 There remain several unanswered questions, however, concerning the roles of PY motifs in

89 Comm function and the mechanistic relationship between Comm, Robo1, and Nedd4 family
90 members during midline crossing in the embryonic nerve cord.
91 Firstly, it is debated whether Comm must be ubiquitinated by Nedd4-family ligases to
92 effectively downregulate Robo1, as two previous studies investigating this question generated
93 contradictory results. The first study demonstrated that Nedd4 ubiquitinated Comm, and that
94 Comm required both its PY motifs and its cytoplasmic ubiquitin-accepting lysines to direct
95 Robo1 to endosomes and downregulate its surface expression in cell culture (Myat et al., 2002).
96 Interestingly, in the second study, an un-ubiquitinatable Comm mutant (Comm KR with all
97 ubiquitin-accepting lysines mutated to arginines) was undistinguishable from wild-type Comm in
98 its ability to localize itself and Robo1 to endosomes *in vitro* and induce Comm gain-of-function
99 phenotypes *in vivo* (Keleman et al., 2005). In addition, it remains unknown whether Nedd4-
100 family ligases are involved in midline crossing. When stained with a pan-neuronal marker,
101 embryos homozygous for a chromosomal deletion that removes Nedd-4 had no noticeable
102 defects in commissural axon guidance (Keleman et al., 2005). This finding alone, however, is
103 insufficient to rule out a role for Nedd4 in midline crossing due to the possibility that loss of
104 function effects could be masked by maternal deposition of Nedd-4, and/or possible redundancy
105 with the other *Drosophila* Nedd4-family ligases Smurf and Su(dx).
106 In this study, we characterize the roles of PY motifs in Comm function and elucidate the
107 mechanistic relationship between Comm, Robo1, and Nedd4-family ligases during midline
108 crossing. To do this, we generated variants of Comm in which the LPSY motif (1PY) or both PY
109 motifs (2PY) are mutated and examined the effects of PY motif disruption on various Comm
110 functions. In contrast to previous literature, we find that mutating the Comm LPSY motif alone
111 does not completely disrupt proper localization to late endosomes *in vitro* and *in vivo*, direction
112 of Robo1 away from the cell surface, and promotion of midline crossing. In addition, while
113 previous studies only assayed the ubiquitination of Comm itself, we demonstrate that PY motifs
114 are necessary for Comm to facilitate Robo1 ubiquitination and lysosomal degradation. Due to

115 the importance of PY motifs for Comm function, we also investigated whether any of the three
116 Drosophila Nedd4-family ligases play a role in midline crossing. Using sensitized genetic
117 backgrounds, we provide evidence that loss of Nedd4, but not Smurf or Su(dx), lead to midline
118 crossing defects in the embryonic nerve cord. In addition, we observe that Comm, Robo1, and
119 Nedd4 interact as a three-member complex and that Comm PY motifs are necessary for Nedd4
120 incorporation into this complex. Finally, we demonstrate that exogenous Nedd4 enhances the
121 ability of Comm to downregulate Robo protein levels *in vivo*. Taken together, these findings
122 support a model in which Comm acts as a substrate adaptor to bring Robo1 into proximity to
123 Nedd4, which it recruits via its PY motifs. This adaptor activity then allows Nedd4 to ubiquitinate
124 Robo1, shunting it away from the growth cone membrane and to late endosomes and
125 lysosomes for degradation. Finally, the resulting downregulation of Robo1 surface levels
126 renders commissural axons insensitive to repulsive slit signals, allowing for midline crossing. In
127 addition to providing new insights into the mechanism of Comm function, the work in this study
128 reconciles two previously conflicting lines of research. Both earlier studies of Comm identified
129 important aspects of Comm function, and by investigating key features of the conflicting models,
130 we were able to unify them into a single coherent picture.
131

132 **Results**

133 **The PY motifs of Comm are required to promote midline crossing *in vivo***

134 As a first step to investigate the relationship between Comm and Nedd4-family ubiquitin
135 ligases, we tested the roles of two putative Nedd4-family ligase binding sites in Comm's
136 cytoplasmic tail: the PY motifs PPCY at amino acid positions 220-223 and LPSY at amino acid
137 positions 229-232. Previous studies have demonstrated the necessity of these PY motifs for
138 Comm's ability to promote midline crossing in vivo (Keleman et al., 2002; Myat et al., 2002);
139 however, the previous studies used random insertions of Comm transgenes, making it very
140 difficult to directly compare the *in vivo* activities of different mutant variants of the Comm protein.

141 To circumvent this issue, we generated transgenic flies carrying UAS transgenes of the
142 following three Comm variants: WT (Wild-type), 1PY (LPSY->AASY), and 2PY (PPCY->AACY,
143 LPSY AASY, Figure 1A), and inserted them into the same integration site on the third
144 chromosome to ensure that these transgenic flies expressed equivalent levels of Comm
145 transcripts when crossed to flies bearing neuronal gal4 drivers. To allow us to vary the
146 expression levels of these different Comm variants, we created two sets of transgenic flies. In
147 the first set, we cloned the Comm coding sequence downstream of 5 copies of the UAS
148 promoter sequence (5X-UAS) and in the second set we used 10 copies of the UAS sequence
149 (10X-UAS). We then assayed the ability of the variants to induce misrouting of ipsilateral axons
150 across the midline in the embryonic nerve cord. In these assays, we examine the eight
151 posterior-most segments of the nerve cord, which are each comprised of an anterior and
152 posterior commissure or 16 total commissures. First, we expressed these 5X-UAS variants
153 under the pan-neuronal Elav-gal4 driver, and investigated their effect on FasII neurons, which
154 run in three parallel ipsilateral bundles along the longitudinal tracts of the nerve cord (Figure
155 1B). We found that WT Comm induced ectopic FAS II crossing in roughly half the commissures
156 in the nerve cord (mean=52%, n=17). In contrast to previously published data, Comm 1PY was
157 also able to induce ectopic FAS II crossing, though it was significantly less effective than WT
158 ($p<0.0001$, ANOVA/Tukey, n=23). Finally, nerve cords of embryos expressing Comm 2PY were
159 indistinguishable from those of control embryos not carrying any Comm transgenes ($p=0.997$,
160 ANOVA/Tukey, 2PY n=20, CTRL n=18) (Figure 1B, C).
161 To investigate the ability of Comm to induce ectopic midline crossing in a cell-
162 autonomous manner, we expressed Comm variants in apterous neurons using the apGal4
163 driver and investigated their effect on this specific ipsilateral neuron population. The apGal4
164 element is expressed in only three neurons per hemisegment allowing for greater resolution of
165 midline crossing phenotypes. We observed that Comm expression induces ectopic apterous
166 crossing in the anterior commissure of nerve cord segments. Nearly all nerve cord segments of

167 embryos expressing WT Comm had ectopic apterous crossing events (mean=85.28%, n=29).
168 Consistent with our FasII data, Comm 1PY induced significantly fewer ectopic crossing events
169 than WT, and Comm 2PY was completely unable to induce ectopic crossing (Figure 1D, E).
170 As expected, expressing higher levels of WT Comm using 10X-UAS results in a much
171 more severe ectopic crossing phenotype; indeed, these embryos have a *slit* mutant phenotype
172 (Figure S1). Surprisingly, we observed that pan neural expression of 10X Comm-2PY, which
173 has no effect when expressed at lower levels, leads to a striking gain of function phenotype
174 where many segments display strong ectopic crossing, both with FasII and with HRP (Figure
175 S1). Taken together, these data indicate that intact PY motifs play an important and a dose-
176 dependent role in Comm's ability to induce midline crossing and raise the possibility that Comm
177 may also inhibit midline repulsion independently of its PY motifs.

178 **Comm PY motifs are required for Robo1 ubiquitination and lysosomal degradation**

179 *In vivo*, Comm overexpression has been shown to reduce Robo1 protein levels and
180 produces a phenotype characterized by excessive midline crossing, reminiscent of the Robo1
181 loss-of-function phenotype (Kidd et al., 1998). However, previous studies have not investigated
182 the mechanism underlying Robo1 protein degradation. To determine the role of Comm PY
183 motifs in reducing Robo1 protein levels and to define the degradative mechanism, we co-
184 expressed Robo1 and Comm variants in S2R+ cells, and measured the expression of both
185 Comm and Robo1 by quantitative Western blotting. We found that co-expression of WT comm
186 significantly reduces Robo1 levels compared to those in cells transfected with Robo1 alone
187 (Figure 2A, B). Comm 1PY also reduces Robo1 levels, though it is significantly less effective at
188 doing so than WT Comm, while Comm 2PY is completely unable to reduce Robo1 levels
189 (Figure 2A, B). Interestingly, mutating the PY motifs in Comm also affects stability of the Comm
190 protein itself. Levels of Comm 1PY and 2PY are elevated relative to WT Comm (Figure 2A, C).
191 Taken together, these findings suggest that PY motifs are critical for turnover of the Comm
192 protein, as well as its ability to facilitate Robo1 degradation.

193 Since PY motifs can act as binding sites for Nedd4-family ubiquitin ligases (Kanelis et
194 al., 2006; Kanelis et al., 2001; Kasanov et al., 2001), we next investigated whether ubiquitination
195 plays a role in regulating Robo and Comm protein stability. Previous studies demonstrated that
196 Comm is ubiquitinated (Myat et al., 2002), but this ubiquitination appears to be dispensable for
197 its function including proper localization, and promotion of midline crossing, since mutation of all
198 of Comm's cytoplasmic lysines (Comm KR) has no apparent effect on its localization or function
199 (Keleman et al., 2005). Somewhat surprisingly, the possibility that Comm facilitates Robo1
200 ubiquitination was never investigated. This led us to evaluate the possibility that Comm
201 downregulates Robo1 levels by facilitating Robo1 ubiquitination and therefore, leading to its
202 degradation. To test whether Comm facilitates Robo ubiquitination, we co-transfected S2R+
203 cells with Robo1 and the Comm variants along with a construct expressing Flag-tagged
204 ubiquitin, and then immunoprecipitated Robo1 and assessed its ubiquitination levels (Figure 2D,
205 E). WT Comm significantly increases Robo1 ubiquitination levels relative to those observed in
206 cells transfected with Robo1 alone and removing either LPSY or both PY motifs eliminates
207 Comm's ability to enhance Robo1 ubiquitination (Figure 2D, E). Importantly, in cells co
208 transfected with Robo1 and WT Comm, treatment with the lysosomal inhibitor chloroquine
209 significantly stabilizes ubiquitinated Robo1 (Figure 2D, E). Taken together our results show that
210 Comm facilitates Robo1 ubiquitination in a PY motif-dependent manner and this ubiquitinated
211 Robo1 is degraded in the lysosome.
212 To test the effects of expressing Comm on Robo protein levels *in vivo*, we measured the
213 expression of endogenous Robo1 protein in embryos over-expressing 5X UAS Comm
214 transgenes by quantitative immunofluorescence (Figure 3). In stage 15-16 embryos,
215 endogenous Robo is expressed at high levels in the longitudinal portions of the axon scaffold
216 and is largely absent from the commissural portions of projecting axons (Figure 3Ai).
217 Overexpression of WT comm under the elavGal4 driver significantly reduces endogenous
218 Robo1 levels (Figure 3Aii, B). As predicted from our *in* vitro data, loss of one PY motif

219 significantly diminished Comm's ability to downregulate Robo1 levels, while loss of both
220 eliminated the ability altogether and endogenous Robo1 levels are indistinguishable from control
221 embryos (Figure 3Aii, B). Since expression of high levels of Comm 2PY with elavGal4 (10x-
222 UAS-Figure S1) is still able to induce significant ectopic midline crossing, we were curious
223 whether endogenous Robo1 levels are also reduced in embryos over expressing 10X-UAS
224 Comm 2PY. Intriguingly, while expression of either 10X-UAS Comm WT or Comm 1PY leads to
225 even stronger reduction in endogenous Robo1 than the 5X transgenes, expression of 10X-UAS
226 Comm 2PY does not reduce endogenous Robo1 levels at all (Figure S2A, B). We also tested
227 the effects of mutating the PY motifs on the expression of the Comm protein itself, and
228 consistent with our *in vitro* experiments, we find that loss of PY motifs increases Comm levels in
229 a dose-dependent manner (Figure 3A, C). Interestingly, even when over-expressed using the
230 Gal4-UAS system, Comm is barely detected unless the PY motifs are mutated. Taken together,
231 these data suggest that PY motifs control the stability of the Comm protein, as well as its ability
232 to facilitate Robo1 degradation. In addition, our observation that expression of 10X-UAS Comm
233 2PY does not reduce endogenous Robo1 levels suggests that in the absence of its PY motifs,
234 Comm can still inhibit midline repulsion and that this effect is not due to reduced levels of Robo
235 1 protein (see discussion).

236 **The PY motifs of Comm act cooperatively to regulate Comm and Robo1 localization**

237 As Comm has been proposed to promote midline crossing by preventing Robo1 from
238 reaching the growth cone surface (Keleman et al., 2002; Keleman et al., 2005), we next
239 investigated the involvement of PY motifs in the intracellular localization of both Comm and
240 Robo1. Previous studies used mammalian COS-7 cells to examine Comm's effect on Robo1
241 localization because of their large size and spread morphology (Keleman et al., 2002; Keleman
242 et al., 2005); thus, to allow comparison with the earlier studies, we first co-transfected COS-7
243 cells with HA-Robo1 and Myc-Comm variants and performed immunostaining for each to
244 visualize their localization. In cells transfected with Robo1 alone, Robo1 is diffusely localized

245 throughout the cell, in intracellular puncta, and at the cell surface (Figure 4A). As observed in
246 previous studies (Keleman et al., 2002; Keleman et al., 2005; Myat et al., 2002), when co-
247 transfected with WT Comm, we see a dramatic change in Robo1 localization. Instead of diffuse
248 localization throughout the cell, Robo1 is predominantly found with Comm in intracellular puncta
249 (Figure 4A, B). In contrast to previous findings (Keleman et al., 2002), disruption of the LPSY
250 motif alone (Comm 1PY) does not alter Comm localization compared to WT; however, Comm
251 1PY is significantly less effective at routing Robo1 to intracellular puncta, and we observe a
252 return of diffuse Robo1 expression (Figure 4A-C). In contrast to Comm 1PY, Comm2PY shows
253 diffuse localization throughout the cell, as well as impaired ability to route Robo1 to intracellular
254 puncta. In summary, the LPSY motif is dispensable for proper Comm localization in cell culture
255 but is required for effective routing of Robo1, while loss of both PY motifs, causes Comm mis-
256 localization as well as a failure to recruit Robo1 to intracellular puncta.

257 To explore the ability of Comm to regulate the surface expression of Robo1 and to
258 further evaluate the importance of the PY motifs in this context, we performed a series of
259 experiments in live dissected unpermeabilized stage 15 embryos. This method allows us to
260 detect the amount of endogenous Robo1 that is present on the axonal surface in various
261 genetic backgrounds. In control embryos, Robo1 is present on the surface of longitudinal
262 portions of axons in the developing ventral nerve cord (Figure 4D). In contrast, minimal Robo1 is
263 detected on the axonal surface in embryos expressing 5X UAS wild-type Comm (Figure 4D). In
264 embryos expressing 5X UAS Comm 2PY, Robo1 is expressed normally on the axonal surface.
265 These observations support our localization studies in COS-7 cells and suggest that Comm can
266 prevent Robo1 surface expression *in vivo.*

267 **Comm can recruit Robo1 to late endosomes *in vivo***

268 To further investigate the role of PY motifs in Comm localization *in vivo*, and to define
269 the subcellular localization of Comm, we ectopically expressed UAS transgenes of the Comm
270 variants using the apGal4 driver. Although ap neurons are ipsilateral and do not express

271 endogenous Comm, they are a small and sufficiently sparse neuronal population to allow for
272 easy visualization of both axons and cell bodies. We found that WT Comm is restricted to cell
273 bodies and displays a punctate expression pattern indicative of localization in intracellular
274 vesicles (Figure 5A, B). Like WT Comm, Comm 1PY is observed in cell body puncta. However,
275 Comm 1PY, unlike WT Comm, is also present in axons. Comm 2PY displays even greater
276 enrichment in axons (Figure 5A, B). The observation that mutating Comm PY motifs leads to a
277 dose-dependent increase in axonal localization of Comm, coupled with a failure of these
278 mutants to down-regulate Robo1 and promote midline crossing strongly suggest that the
279 primary site of Comm function is in the cell soma. As most actively degradative intracellular
280 compartments are restricted to the soma in neurons (for a review of the neuronal
281 endolysosomal system, see (Roney et al., 2022)), these findings support the role of PY motifs
282 for routing Comm and its cargo to late endosomes and lysosomes.

283 To determine whether Comm localizes to late endosomes and lysosomes, we co-
284 expressed Comm variants with GFP-tagged late endosomal/lysosomal markers using apGal4.
285 Two such markers, Rab7 and Lamp1, are observed in a punctate pattern within cell bodies but,
286 as expected, are largely excluded from axons when overexpressed in apterous neurons (Figure
287 5C-E and Figure S3). Each Comm variant can be observed in puncta positive for Rab7 or
288 Lamp1; however, both Comm PY mutant variants show a significant reduction in total co-
289 localization with these late endosomal and lysosomal markers relative to wild-type Comm
290 (Figure 5 C-E, $p<0.05$ for both 1PY and 2PY, ANOVA). This reduction is largely due to the fact
291 that axonally localized Comm 1PY or 2PY does not co-localize with either marker (Figure 5C-E
292 and Figure S3). Interestingly, PY mutant Comm variants show significantly less co-localization
293 with Lamp1 even when only observing Comm present in cell bodies, suggesting that with
294 Lamp1, total co-localization is not only decreased due to Comm leakage into axons, but also
295 due to compromised routing to the correct subcellular compartments within cell bodies (Fig 5C,
296 E). Collectively, these findings demonstrate that Comm localizes to late endosomes and

297 lysosomes *in vivo* and that PY motifs keep Comm restricted to these compartments. In
298 summary, PY motifs are critical for proper localization of Comm to degradative compartments
299 and its ability to route its cargo Robo1 away from the cell surface.

300 **Nedd4 promotes midline crossing of commissural axons**

301 In the experiments described, we have demonstrated the importance of PY motifs for
302 numerous Comm functional outputs: promotion of midline crossing, targeting to
303 endosomes/lysosomes, Robo trafficking, and promotion of Robo ubiquitination and degradation.
304 As these motifs are known to bind Nedd4-family ubiquitin ligases and are indispensable for
305 Comm function, we investigated whether any of the Nedd4-family ligases play a role in midline
306 crossing *in vivo*. Previous studies have led to conflicting conclusions about the importance of
307 Nedd4 for midline crossing. One study found that Nedd4 overexpression increases the Comm
308 gain-of-function phenotype characterized by ectopic midline crossing (Myat et al., 2002);
309 however, a different research group was unable to replicate these results and also observed
310 that embryos homozygous for a chromosomal deletion covering the Nedd4 locus show no
311 obvious midline crossing defects (Keleman et al., 2005). These results call into question the role
312 of Nedd4 in midline crossing. Given our biochemical results showing that Comm promotes
313 Robo1 ubiquitination through its predicted Nedd4 binding sites and the potential redundancy
314 among the three Drosophila Nedd4 family ligases, we revisited the role of Nedd4 ubiquitin
315 ligases in commissural axon guidance and in the regulation of Robo1 using genetic and
316 biochemical approaches.

317 To evaluate a potential role for Nedd4 in midline crossing, we first examined its
318 expression pattern in developing embryos using a Mimic insertion (Nagarkar-Jaiswal et al.,
319 2015), which inserts a GFP tag into the coding sequence of the endogenous Nedd4 locus
320 (Nedd4-GFP). Using this tool, we observe a strong enrichment of Nedd4 protein in the ventral
321 nerve cord of stage 14 embryos, a stage when many commissural axons are extending across
322 the midline. Using this line, we are able to detect Nedd4 protein in both cell bodies and CNS

323 axons, indicating that Nedd4 is present at the right time and place to play a role in commissural
324 axon guidance (Figure S4). To test for a functional role of Nedd4 in midline guidance, we used
325 the well-characterized Nedd4T119FS allele, which was generated via EMS mutagenesis and
326 induces a frameshift mutation at the 119th amino acid. This frameshift truncates the Nedd4
327 protein, such that it lacks its WW (PY-motif binding) domains and HECT ubiquitin ligase domain,
328 which renders it non-functional (Sakata et al., 2004). When we examined embryos homozygous
329 for this loss of function allele with HRP immunofluorescence, we detected no obvious defects
330 (Figure 6A), consistent prior observations using a chromosomal deletion for Nedd4 (Keleman et
331 al., 2005). Since Nedd4 transcript is known to be maternally deposited, we sought to further limit
332 Nedd4 function by generating maternal/zygotic mutants. However, these approaches were not
333 successful, presumably due to the necessity of Nedd4-family ligases in oogenesis (Xia et al.,
334 2010) as well as early patterning events and cell fate decisions that occur before axon guidance
335 begins. ((Bakkers et al., 2005; Lin et al., 2017; Lohraseb et al., 2022; Persaud et al., 2011;
336 Podos et al., 2001; Zhang et al., 2014)).
337 To more thoroughly examine if Nedd4 plays any role in commissural axon guidance, we
338 used two sensitized genetic backgrounds that lead to partial disruptions in midline crossing,
339 *frazzled* loss of function mutants and ecotopic expression of a truncated Frazzled receptor,
340 Fra∆C (Garbe et al., 2007). We and others have used these genetic backgrounds to
341 demonstrate important functional roles for a number of genes in commissural axon guidance
342 that are otherwise undetectable, including Robo2 and the transmembrane and secreted
343 Semaphorins (Sema1a and Sema2A, B respectively) (Arbeille and Bashaw, 2018; Evans et al.,
344 2015; Hernandez-Fleming et al., 2017; Spitzweck et al., 2010). In *fra* mutants there are
345 significant disruptions in midline crossing that can be observed when visualizing the entire axon
346 scaffold as well as when visualizing a subset of commissural axons (labeled by egGal4
347 expressing CD8-GFP). Specifically, *fra* mutants display thin or missing posterior commissures in
348 approximately 30% of embryonic segments. In egGal4-expressing commissural neurons, the

349 EW cluster of neurons normally project across the posterior commissure and approximately
350 35% of EW neurons fail to project their axons across the midline in *fra* mutants (Figure 6A-D).
351 While removing one copy of Nedd4 does not increase crossing defects in the *fra*-null
352 background, as measured by commissure thickness with HRP (Figure 6A, B) or EW crossing
353 (Figure 6C, D), removing both copies of Nedd4 leads to a significant enhancement of the *fra*
354 mutant phenotype, and a profound disruption in midline crossing, in some instances resembling
355 *comm* loss of function mutants (Figure 6A). *fra, nedd4* double mutant embryos are missing over
356 half of their commissures (compared to the <10% missing in fra single mutants) and most of the
357 remaining commissures are thin (Figure 6A, B). These defects are also observed in the anterior
358 commissure, a phenotype that is never observed in *fra* mutants alone. The crossing defects of
359 the eagle neurons are also significantly increased and include defects in the projection of Eg
360 neurons through the anterior commissure (Figure 6C, D). These observations indicate that
361 *Nedd4* acts in parallel to *fra* to promote commissural axon growth across the midline.
362 To further support these observations, we also examined the consequences of removing
363 *nedd4* In the FraΔC background. Expression of FraΔC using the egGal4 driver induces EW
364 crossing defects in 30-50% of abdominal segments but does not affect EG neuron crossing.
365 While Nedd4 heterozygotes show no alterations in commissural axon guidance defects in the
366 FraΔC background, Nedd4 homozygous mutants display significantly increased EW non-
367 crossing phenotypes. We were able to take advantage of this genetic interaction to test for a
368 neuron-autonomous function of Nedd4 by performing rescue experiments. We find that
369 expressing a UAS Nedd4 transgene in embryos homozygous mutant for *nedd4* in the FraΔC
370 background leads to a significant reduction in the non-crossing defects (Figure 6 E, F). Taken
371 together, these results demonstrate an important role for Nedd4 in promoting midline crossing
372 and suggest that it functions cell autonomously in neurons.
373 **Smurf and Su(dx) are dispensable for midline crossing**

374 There are three Nedd4 family E3 ubiquitin ligases in *Drosophila:* Nedd4, Smurf and
375 Su(Dx). To investigate whether Smurf and Su(dx) could also play a role in midline crossing, we
376 first examined their expression patterns by searching the embryonic mRNA expression data
377 base of the Berkeley Drosophila Genome Project (BDGP). This database includes images of
378 mRNA *in situ* patterns for many fly genes. Data reported for Su(Dx) show that it is expressed
379 broadly or ubiquitously throughout all stages of embryogenesis including in the nerve cord of
380 stages 14 through 16 embryos. No data is publicly available for Smurf, so we generated our
381 own *in situ* probes to visualize the Smurf embryonic mRNA expression pattern and found that
382 like Su(Dx), Smurf is broadly expressed during embryogenesis, including in the developing
383 nerve cord (Figure S4). Thus, although Su(Dx) and Smurf do not show striking nerve cord
384 enrichment like Nedd4, their expression patterns are consistent with potential roles in
385 commissural axon guidance.
386 To investigate roles for Smurf and Su(Dx) in midline axon guidance, we examined the
387 nerve cords of embryos lacking functional copies of each gene. We used the Smurf 15C loss-of-
388 function allele, generated by insertion of a hobo element which disrupts the coding sequence of
389 its HECT domain (Podos et al., 2001), and the deficiency line Df(2L)Exel7008 which contains
390 the smallest available chromosomal deletion covering the Su(dx) locus. Similar to *nedd4*
391 mutants, zygotic loss of either Smurf or Su(dx) function produced no visible midline crossing
392 defects in nerve cords stained with the pan-neuronal marker HRP (Figure S5A, B and S6A, B).
393 Due to potential effects of maternal deposition and possible redundancy, we next investigated
394 whether loss of Smurf or Su(dx) could induce midline crossing defects in the *fra* mutant and
395 Fra∆C sensitized genetic backgrounds as described above for our investigation of *nedd4*. In
396 marked contrast to our findings with *nedd4*, removing both zygotic copies of either *smurf* or
397 *su(dx)* does not increase the occurrence of EW non-crossing in either *fra* mutant embryos or in
398 embryos expressing Fra∆C using egGal4. Based on these findings, it is unlikely that either
399 ligase plays a major role in midline crossing; however, we cannot rule out the possibility that

400 either Smurf or Su(Dx) acts redundantly with Nedd4. Nevertheless, our genetic experiments are
401 most consistent with Nedd4 playing the prominent role in regulating midline crossing.

402 **Nedd4 interacts with the slit/Robo pathway both biochemically and genetically**

403 Our observations that Comm facilitates Robo1 ubiquitination and lysosomal degradation
404 through its cytoplasmic PY motifs, together with our genetic data showing that *Nedd4* promotes
405 commissural axon guidance across the midline, suggest that Comm and Nedd4 function
406 together to inhibit Robo1 repulsion. If indeed, Comm serves as a substrate adapter to allow
407 Nedd4 to target Robo1 for ubiquitination and subsequent degradation, we reasoned that the
408 three proteins should form a complex. Furthermore, we predicted that in the absence of Comm
409 or when the PY motifs of Comm are mutated, Nedd4 should exhibit reduced association with the
410 Robo1 receptor. To test these predictions, we performed a series of coimmunoprecipitation
411 experiments in S2R+ cells. When Robo1 and Nedd4 are co-transfected in the absence of
412 Comm, we detect very little if any association between Nedd4 and Robo1 (Figure 7A).
413 Strikingly, when all three proteins are expressed, Nedd4 readily co-precipitates with Robo1,
414 even though the presence of Comm greatly reduces Robo1 protein levels (Figure 7A). As
415 predicted, mutating the PY motifs leads to a significant decrease in the amount of Nedd4 that is
416 incorporated into the complex, even though the level of Robo1 protein expression increases
417 when Comm PY motifs are mutated (Figure 7B). Both observations are consistent with the
418 model that Comm acts as a substrate adapter between Nedd4 and Robo1 (Figure 7C).

419 To determine whether Nedd4 can function together with Comm *in vivo* to downregulate
420 the expression of the Robo1 receptor, we measured the expression level of endogenous Robo1
421 protein biochemically in wild-type embryos, embryos expressing transgenic Comm, or embryos
422 expressing both Comm and Nedd4. We collected protein lysates from these three groups of
423 embryos that were aged between 13 – 18 hours post-fertilization, since this is developmental
424 window when axons in the CNS are actively growing toward their targets. As predicted from our
425 *in vitro* measurements of the effect of Comm on Robo1 expression levels, pan-neural

426 expression of Comm leads to a striking reduction in Robo1 protein levels. Importantly this effect
427 is significantly enhanced in embryos co-expressing Comm and Nedd4 (Figure 7D, E), which
428 further supports the idea the Nedd4 facilitates Comm-dependent Robo1 degradation.
429 Interestingly, and consistent with our *in vitro* biochemistry, co-expression of Nedd4 and Comm
430 also leads to reduced levels of Comm protein relative to embryos expressing Comm alone,
431 suggesting that Comm, like Robo1 is likely degraded by Nedd4 (Figure 7E, see discussion).
432 While these observations strongly support the idea that Nedd4 can work with Comm to
433 downregulate Robo1 protein levels *in vivo,* they do not allow us to make conclusions about
434 where Robo1 levels are decreasing. To address this question, we monitored endogenous
435 Robo1 levels in these embryos by immunofluorescence to determine if co-expression of Comm
436 and Nedd4 leads to reduction in the axonal expression or Robo1. Consistent with the data
437 presented in earlier (Figures 3, 4 and S2), ectopic expression of Comm results in a striking
438 decrease in axonal Robo1 expression. Importantly, axonal Robo1 levels are further reduced
439 when Nedd4 is co-expressed with Comm (Figure 7F-G). Taken together, these findings support
440 a model in which Comm recruits Nedd4 via its PY motifs, bringing it into proximity with Robo1,
441 facilitating its ubiquitination, localization to late endosomes/lysosomes, and ultimately its
442 lysosomal degradation (Figure 8).
443

444 **Discussion**

445 The data presented here support a model that is a hybrid of the two developed
446 previously (Keleman et al., 2005; Myat et al., 2002), in which Comm requires interaction with
447 Nedd4 to downregulate Robo1, and in which Robo1, not Comm, is the primary substrate for
448 Nedd4 ubiquitination. Through a combination of *in vivo* and *in-vitro* experiments, we
449 demonstrate that Comm requires intact PY motifs to localize effectively to late
450 endosomes/lysosomes, route Robo1 away from the cell surface, facilitate Robo1 ubiquitination
451 and degradation, and enable midline crossing. We also find that Comm lacking one or both of its

452 PY motifs is more stable than its wild-type counterpart. Using *in-vitro* biochemical assays, we
453 show that Nedd4 is recruited into a ternary complex with Comm and Robo1 in a manner
454 dependent on Comm PY motifs. In addition, *in-vivo* loss and gain-of-function experiments
455 indicate a specific and cell-autonomous role for Nedd4, but not other Nedd4 family members
456 Su(dx) and Smurf, in midline crossing. Finally, we show that overexpression of Nedd4 enhances
457 downregulation of Robo1 levels by Comm *in vivo*, as well as turnover of the Comm protein itself.
458 Taken together, these findings support a model of Robo1 downregulation in which Comm acts
459 as an adaptor protein between Robo1 and Nedd4, recruiting Nedd4 into a three-member
460 complex with itself and Robo1 via its PY motifs. Once the two proteins are close to one another,
461 Nedd4 can ubiquitinate Robo1, leading to lysosomal trafficking and degradation of the entire
462 complex and ultimately, inhibition of premature Robo1-mediated repulsion at the growth cone
463 (Figure 8).

464 **New insights into the role of PY motifs in Comm Function**

465 In accordance with previous studies (Keleman et al., 2002; Myat et al., 2002), we find
466 that PY motifs are necessary for Comm to promote ectopic midline crossing in ipsilateral neuron
467 populations and to promote Comm localization to intracellular puncta *in vitro*. One study had
468 reported that mutation of the LPSY motif alone completely disrupts both Comm's ability to
469 promote ectopic crossing and its localization to presumptive endosomes in cultured cells
470 (Keleman et al., 2002). In contrast, by directly comparing Comm transgenes inserted in the
471 same genetic locus, we were able to dissect the relative roles of these motifs and show that the
472 PY motifs act in an additive manner, as disruption of the LPSY motif alone and both PY motifs
473 disrupted Comm's ability to promote midline crossing in a dose-dependent manner. Our
474 experiments *in vitro* further support an additive role for the PY motifs in controlling Comm and
475 Robo1 localization and suggest distinct activities of the two motifs. Specifically, we observe that
476 while Comm 2PY is unable to efficiently localize itself or Robo1 to intracellular puncta in COS-7
477 cells, Comm lacking only the LPSY motif itself localizes normally, but it is compromised in its

478 ability to route Robo to puncta along with it. This suggests the interesting possibility that there
479 may be instances when Comm and Robo can separate during intracellular trafficking. We
480 further dissected the structural requirements for Comm localization *in vivo*, where we found that
481 disruption of Comm PY motifs causes “leakage” of Comm from cell bodies into axons in a dose-
482 dependent manner. These observations suggest that PY motifs are required to shunt Robo
483 away from the growth cone and this possibility is further supported by our finding that Comm
484 lacking functional PY motifs is unable to reduce the expression of Robo on the surface of
485 commissural axons *in vivo*. Finally, we demonstrate that mutation of the LPSY or both PY motifs
486 compromises colocalization of Comm and Lamp1+ puncta, showing that PY motifs are required
487 for trafficking to late endosomes and lysosomes *in vivo*.

488 In addition to localization, our work offers important new insights into how Comm
489 downregulates Robo1 protein levels. Both *in vivo* and *in vitro*, we find that disrupting Comm PY
490 motifs inhibits its ability to promote Robo1 degradation. Biochemical assays demonstrate that
491 Comm requires PY motifs to recruit Nedd4 into a complex with itself and Robo1 and promote
492 Robo ubiquitination. As ubiquitinated Robo1 is stabilized by chloroquine, our results show that
493 Comm facilitates the degradation of this pool of Robo1 via a lysosomal pathway. Taken
494 together, these observations implicate PY motifs as major players in all known aspects of
495 Comm function: localization to late endosomes, ability to regulate localization and protein levels
496 of its cargo, and promotion of midline crossing.

497 **Robo1 is a substrate for Nedd4 ubiquitination**

498 Comm has been shown to be ubiquitinated in the presence of Nedd4 (Myat et al., 2002);
499 however, the importance of ubiquitination for Comm function has been cast into doubt by the
500 findings that an un-ubiquitinatable form of Comm (Comm KR) is able to localize correctly and
501 traffic Robo1 to intracellular puncta in COS-7 cells, and promote midline crossing *in vivo* as
502 effectively as WT Comm (Keleman et al., 2005). Despite these observations and studies
503 implicating ubiquitination as a negative regulator of Robo1 repulsion (Yuasa-Kawada et al.,

504 2009), the possibility that Comm facilitates ubiquitination of its cargo Robo1 has not yet been
505 explored. We found that in the presence of Comm, Robo1 ubiquitination is significantly
506 increased, and that mutation of Comm PY motifs prevents this increase. This, combined with
507 the observation that the addition of exogenous Nedd4 leads to a further reduction of Robo1
508 protein levels by Comm, supports a model in which Comm downregulates Robo1 by recruiting
509 Nedd4 through its PY motifs to trigger Robo1 ubiquitination and subsequent lysosomal
510 degradation. In our biochemical assays, mutation of Comm PY motifs not only impedes
511 downregulation of Robo1 protein levels but also increases the stability of Nedd4 (Fig 7Aii) and
512 Comm, suggesting that these three proteins are trafficked to the lysosome and degraded
513 together as a complex.
514
515 **Nedd4 is the primary member of the Nedd4 family involved in midline crossing**
516 Prior studies had generated contradictory findings concerning the role for Nedd4 in
517 midline axon guidance. Here, we provide conclusive evidence of a role for Nedd4 in promoting
518 midline crossing by showing that loss of *nedd4* increases crossing defects in the fraΔc or fra-/-
519 sensitized genetic backgrounds. Further, we show that in the fraΔc background, re-expression
520 of transgenic Nedd4 in a the Eg subset of commissural neurons rescues the midline crossing
521 defects, indicating a likely cell autonomous role for Nedd4 in this process. In contrast, zygotic
522 mutation of either Su(dx) or Smurf did not result in midline axon guidance defects in wild-type
523 embryos or in either of these sensitized genetic backgrounds. While we were unable to show
524 evidence of a role for Su(dx) and Smurf through genetic assays in sensitized backgrounds, we
525 still have insufficient evidence to definitively rule out a role for them. Many of the factors
526 prompting us to use sensitized backgrounds, especially maternal expression and redundancy
527 among Nedd4 family members, present us with significant challenges in detecting loss of
528 function phenotypes. In addition, Nedd4 family E3 ligases regulate several additional pathways
529 involved in critical early-developmental patterning events, including germ layer specification,

530 establishment of major body axes, and fate determination of the neuroectoderm. At least two
531 different Nedd4-family ligases are known to regulate each of the following pathways: Notch,
532 TGF-β, and Wnt (for review see (Ingham et al., 2004)). The fact that none of these pathways are
533 regulated by a sole Nedd4 family E3 ligase suggests that Nedd4 may not be the only Nedd4
534 family member regulating Robo1 and Comm. Unfortunately, the conditions for definitively testing
535 their involvement, such as mutating multiple Nedd4 family members simultaneously or
536 abolishing their maternal expression has not yet been possible.

537 **Comm is likely to regulate Robo1 repulsion through multiple mechanisms**

538 Our data clearly supports an important role for Nedd4 in contributing to Comm's ability to
539 inhibit Robo1 signaling and promote midline crossing; however, several lines of evidence
540 support alternative roles for Comm in preventing midline repulsion. First, a previous study
541 investigated the consequences of generating an endogenously expressed Robo1 receptor that
542 cannot be inhibited by Comm through homologous recombination. Specifically, the coding
543 sequence of Robo1 was replaced by a mutant variant that could not bind to or be
544 downregulated by Comm (termed Robo1-SD for sorting defective)(Gilestro, 2008). If Comm's
545 sole function were to inhibit the surface expression of Robo1, then the prediction would be that
546 these Robo1-SD embryos would phenocopy *comm* mutants; however, quite surprisingly, these
547 embryos appear to be completely normal (Gilestro, 2008). This finding suggests either Comm
548 inhibits the function of another key component of the Slit-Robo1 repulsive pathway, potentially
549 through inhibiting its expression, or alternatively, Comm may inhibit Robo1 function through a
550 second mechanism that is independent of ubiquitin-mediated protein degradation. Since Robo1-
551 SD does not bind to Comm, this alternative mechanism would not depend on binding to Robo1.
552 Our finding that high-level over-expression of the Comm2PY mutant variant that cannot inhibit
553 Robo1 surface expression can still inhibit midline repulsion is consistent with mechanism of
554 regulation that is independent of protein degradation of Robo1, or another Comm substrate.
555 One interesting potential alternative role for Comm would be to prevent Robo1 endocytosis,

556 since receptor endocytosis is required for repulsive signaling (Chance and Bashaw, 2015;
557 Sullivan and Bashaw, 2023). Indeed, at the Drosophila neuromuscular junction (NMJ), Comm
558 has been proposed to regulate endocytosis from the plasma membrane to promote synapse
559 formation (Ing et al., 2007; Wolf et al., 1998).

560 **The role for Nedd4 is evolutionarily conserved**

561 Although we still do not know whether Smurf or Su(dx) play roles in midline crossing, our
562 observation that Nedd4 appears to be the main ligase involved in this process agrees with
563 recent findings in mice and provides additional evidence of a conserved mechanism of Robo1
564 downregulation between vertebrates and invertebrates. While Comm appears to be only present
565 in insects, several vertebrate proteins have been identified that may play analogous roles in
566 mammalian species (Gorla et al., 2019; Justice et al., 2017). Among these proteins that may
567 function analogously to Comm, the Nedd4 family interacting proteins Ndfip1 and Ndfip2 share
568 sequence similarity to the region of Comm containing PY motifs and appear to act as its
569 functional analog in mice. Like Comm, loss of mammalian Ndfip proteins impedes effective
570 midline crossing and results in the upregulation of Robo1 levels in pre-crossing commissural
571 axons in the spinal cord. In addition, Ndfip proteins negatively regulate Robo1 expression in a
572 manner nearly identical to that of Comm: by facilitating Robo1 ubiquitination, diversion away
573 from the cell surface, trafficking to late endosomes, and ultimately, degradation (Gorla et al.,
574 2019).

575 Since these functions of Ndfip proteins rely on functional PY motifs, efforts have been
576 made to determine which of the nine mammalian Nedd4 family E3 ligases they may recruit to
577 regulate Robo1 localization and protein levels. While the seven E3 ligases most related to
578 Drosophila Nedd4 family members can all bind Ndfip proteins *in vitro*, only the Nedd4 homologs
579 Nedd4-1 and Nedd4-2, and the Su(dx) homolog WWP2 can enhance Robo1 ubiquitination and
580 degradation. Unlike the other Nedd4 family ligases tested, Smurf homologs Smurf1 and Smurf2
581 can bind to Ndfip proteins in the absence of functional PY motifs suggesting that they bind to

582 additional structural elements of Ndfip proteins and may be involved in different biological
583 processes. In addition, single and double conditional knockouts of Nedd4-1 and Nedd4- 2
584 display impaired axon guidance across the floor plate of the spinal cord. Taken together, these
585 findings demonstrate an important role for mammalian Nedd4 homologs in commissural axon
586 guidance in the spinal cord (Gorla et al., 2022). The finding that some Nedd4 family members
587 do not facilitate Robo1 ubiquitination and degradation despite binding effectively to Ndfip
588 proteins suggests that additional factors are required to confer substrate specificity to E3
589 ligases. These additional factors appear to be highly cell-type specific, as the same cargo can
590 be ubiquitinated by different E3 ligases in different cellular contexts. For example, Ndfip-
591 mediated ubiquitylation of the divalent metal ion transporter (DMT1) is catalyzed by Nedd4-2 in
592 neuronal cells (Howitt et al., 2009), but is catalyzed by WWP2 in other non-neuronal cell types
593 (Foot et al., 2008; Gorla et al., 2022).. What factors may determine E3 ligase substrate
594 specificity in the developing mammalian and insect CNS remains an open question.
595 Despite the lack of comm homologs outside of insects, the work shown in this paper and
596 the research conducted on Ndfip proteins in the mouse spinal cord point to a common
597 mechanism of Robo1 regulation across species. In both vertebrates and invertebrates, Nedd4
598 substrate adaptor proteins serve as a vital means of downregulating growth cone Robo1 levels
599 by facilitating Robo1 ubiquitination, trafficking to lysosomes, and ultimately, degradation.
600 Discovering additional binding partners for both Comm and Ndfip proteins, especially those
601 shared between both, will be necessary for us to better understand other critical players in this
602 common mechanism. Such binding partners may include proteins involved in determining E3
603 substrate specificity and in trafficking Nedd4 adaptors and their cargoes to the proper
604 destinations. As it is highly likely that Comm regulates other proteins besides Robo1, and Ndfip
605 has several known cargoes in different cell contexts (Foot et al., 2008; Kang et al., 2015; Mund
606 and Pelham, 2010; Trimpert et al., 2017), additional binding partners may also include
607 alternative cargoes of Nedd4 adaptors involved in axon guidance. Such an investigation may

608 offer important insights into how this fundamental Nedd4 substrate adaptor-mediated
609 mechanism to tune the neuronal surface proteome may contribute to development and function
610 of the nervous system.

611

612 **MATERIALS AND METHODS**

613 **Contact for Reagent and Resource Sharing**

614 Further information and requests for resources and reagents should be directed to the Lead
615 Contact, Greg J. Bashaw (gbashaw@pennmedicine.upenn.edu).

616 **Experimental Model and Subject Details**

617 **Genetic stocks**

618 The following *Drosophila* strains were used: *w*^{1118}*, apGal4, egGal4, elavGal4, UAS-CD8GFP II,*
619 *UAS-TauMycGFP III, UAS-fraΔc-HA, fra*^{3}*, nedd4*^{T119FS}*, Mi{PT-GFSTF.0}Nedd4[MI07766-*
620 *GFSTF.0], Df(2R)ED3385, and Df(2R)Excel7008.* The fly strain *smurf*^{15C} was a kind gift from the
621 Pi Lab at Chang Gung University. The following transgenic stocks were generated: *10UAS-*
622 *Comm-myc WT, 10UAS-Comm-myc 1PY, 10UAS-Comm-myc 2PY, 5UAS-Comm-myc WT,*
623 *5UAS-Comm-myc 1PY, 5UAS-Comm-myc 2PY,* and 10UAS-Nedd4-HA. Transgenic flies were
624 generated by Bestgene Inc. (Chino Hills, CA) using PhiC31- directed site-specific integration
625 into landing sites at cytological position 86F8 (For *UAS-Comm* constructs) or 51C (for *UAS-*
626 *Nedd4* constructs). All crosses were carried out at 25°C.

627 **Cell Culture**

628 Drosophila S2R+ cells were maintained at 25°C in Schneider's media (Life Technologies,
629 #21720024) supplemented with 10% (vol/vol) FBS and a mixture of 1% Penicillin and
630 Streptomycin. COS-7 cells were maintained at 37 ^{o}C, 5% CO^{2} in Dulbecco's Modified Eagle

631 Medium (Corning, 10-017-CM) supplemented with 10% (vol/vol) FBS and a mixture of 1%
632 Penicillin and Streptomycin.

633 **Method Details**

634 **Molecular Biology**

635 To make the P10UAST-Comm-myc WT, the WT coding sequence of Comm was PCR amplified
636 and cloned into the *p10UAST-myc* vector described above by swapping out the *hspc300* insert
637 using *Kpn1*/*Asc1* sites and the following primers:

638 Fwd with Kpn1: GCGCGGTACCATGATTAGCACCACGGATTAT

639 Rev with Asc1: AAAGGCGCGCCCGCGGCAACAACAACGA

640 To make the P10UAST-Comm-myc 1PY construct, the LPSY motif of Comm was
641 mutated to AASY via SOE-ing PCR, using the WT Comm coding sequence from P10UAST-
642 Comm-myc WT as a template. The following primers were used to flank the coding sequence
643 and introduce point mutations into the LPSY motif.

644 Fwd with Kpn1: GCGCGGTACCATGATTAGCACCACGGATTAT

645 Rev with Asc1: AAAGGCGCGCCCGCGGCAACAACAACGA

646 LPSY->AASY Fwd: AATCGCCACCGGAGCGGCCAGCTACGATGAGGCACTGCAT

647 LPSY->AASY Rev: ATGCAGTGCCTCATCGTAGCTGGCCGCTCCGGTGGCGATT

648 The resulting Comm 1PY coding sequence was then subcloned back into a n-terminal myc-
649 tagged P10UAST backbone using Kpn1 and Asc1 restriction sites.

650 To generate the P10UAST-Comm-myc 2PY, the coding sequence from P10UAST
651 Comm-myc 1PY was subcloned into the smaller pbluescript backbone. Point mutations were

652 introduced into the PPCY motif using Quikchange II site-directed mutagenesis kit (Agilent,
653 #200523) using the following primers.

654 CAAATCGAATCGGCGGCCTGCTACACAATCGCCACCGGAT

655 ATCCGGTGGCGATTGTGTAGCAGGCCGCCGATTCGATTTG

656 The resulting Comm 1PY coding sequence was then subcloned back into a n-terminal myc-
657 tagged P10UAST c-term myc backbone using Kpn1 and Asc1 restriction sites

658 To generate p5UAST Comm-myc constructs, 5 UAS sites were excised from the
659 P10UAS Comm-myc constructs using the Sph1 restriction enzyme.

660 To generate myc-Comm constructs for transfection in mammalian cells, the coding
661 sequences of WT, 1PY, and 2PY Comm from the P10UAST Comm-myc constructs were
662 subcloned into the pKMyc backbone (Addgene #19400) using the Xba1 and Nhe restriction
663 sites and the following primers:

664 Fwd with Xba1: CCGGTCTAGAATGATTAGCACCACGGATTA

665 Rev with Nhe1: ATAGCTAGCTCACGCGGCAACAACAA

666 To make the P10UAST-FLAG-Ub construct, the FLAG-Ubiquitin coding sequence from a
667 mammalian-expressing Flag-Ub plasmid (cited in (Gorla et al., 2019), originally a kind gift from
668 the Dr. Hideaki Fujitha lab) was subcloned into the P10UAST backbone using Xho1 and Xba1
669 restriction sites. The following primers were used.

670 Fwd with Xho1: AAACTCGAGATGGACTACAAAGACCATGA

671 Rev with Xba1: AAATCTAGATTAACCACCACGAAGTCTCA

672 The P10UAST-Nedd4-HA construct was made by PCR amplifying Nedd4 cdna from the
673 pOT2 DGRC Gold collection (clone SD04682, DGRC Stock 5253) using the following primers.

674 Fwd with Not1: ATATGCGGCCGCATGTCGGCACGTTCCAGC

675 Rev with Kpn1: CCCGGTACCATCAACTCCAGCAAATCCTTGGC

676 The resulting insert was then subcloned into the P10UAST-HA backbone using Not1 and Kpn1
677 restriction sites.

678 **Western Blot**

679 S2R+ cells were transiently transfected with Effectene transfection reagent (Qiagen, Valencia
680 CA, #301425) and induced 24 hours later with 0.5mM copper sulfate. 24 hours after induction,
681 cells were lysed in TBS-V (150 mM NaCl, 10 mM Tris pH-8, 1 mM ortho-vanadate)
682 supplemented with 0.5% Surfact-AMPS NP40 (Thermo, Waltham MA, #85124)) and 1x
683 Complete Protease Inhibitor (Roche, #11697498001) and incubated with agitation for 20 min at
684 4°C. Soluble proteins were recovered by centrifugation at 15,000 rpm for 15 min at 4°C.

685 To collect lysates from *Drosophila* embryos, approximately 100 µl of embryos at the
686 desired developmental stages were treated with 50% bleach (Essendant) for 2 min and washed
687 three times with embryo wash buffer (120 mM NaCl supplemented with 0.1% (v/v) Triton X-100,
688 Sigma). Embryos were then rinsed with ice cold TBSV buffer (150 mM NaCl ,10 mM Tris pH
689 8.0, 2 mM Sodium orthovanadate), and lysed with manual homogenization using plastic pestles
690 in 300 µl lysis buffer (TBSV supplemented with 1% Surfact-AMPS NP40 and 1x complete
691 protease inhibitors). Homogenized samples were then incubated for 30 min at 4 °C with
692 agitation and recovered by centrifugation at 15,000 rpm for 15 min 4 °C.

693 Proteins were resolved by SDS-PAGE and transferred to nitrocellulose membrane
694 (Amersham, #10600032). Membranes were blocked with 5% dry milk and 0.1% Tween 20 in
695 PBS for 1 h at room temperature and incubated with primary antibodies in 2% dry milk/0.1%
696 Tween 20 in PBS overnight at 4°C. Following three washes with PBS/0.1% Tween 20,
697 membranes were incubated with the appropriate HRP-conjugated secondary antibody at room

698 temperature for 1h. Signals were detected using Clarity ECL (Bio-Rad, #1705061) or Super
699 Signal West Femto Maximum Sensitivity Substrate (Thermo Fisher, 34094) according to
700 manufacturer's instructions.

701 **Immunoprecipitation**

702 S2R+ cells were transiently transfected with Effectene transfection reagent (Qiagen, Valencia
703 CA, #301425) and induced 24 hours later with 0.5mM copper sulfate. 24 hours after induction,
704 cells were lysed in TBS-V (150 mM NaCl, 10 mM Tris pH-8, 1 mM ortho-vanadate)
705 supplemented with 0.5% Surfact-AMPS NP40 (Thermo, Waltham MA, #85124) and 1x
706 Complete Protease Inhibitor (Roche, #11697498001) for 20 min at 4°C. Soluble proteins were
707 recovered by centrifugation at 15,000 x g for 10 min at 4°C. Lysates were pre-cleared with 30 µl
708 of a 50% slurry of protein A (Invitrogen, #15918-014) and protein G agarose beads (Invitrogen,
709 #15920-010) by incubation for 20 minutes at 4 ^{o}C. Pre-cleared lysates were then incubated with
710 0.7 µg of rabbit anti-GFP antibody for 2 hours at 4°C to precipitate Robo-GFP. After incubation,
711 30 µl of a 50% slurry of protein A and protein G agarose beads was added and samples were
712 incubated for an additional 30 minutes at 4°C. The immunocomplexes were washed three times
713 with lysis buffer, boiled for 10 min in 2x Laemmli SDS sample buffer (Bio-Rad, #1610737) and
714 analyzed by western blotting. Proteins were resolved by SDS-PAGE and transferred to
715 nitrocellulose membrane (Amersham, #10600032). Membranes were blocked with 5% dry milk
716 and 0.1% Tween 20 in PBS for 1 h at room temperature and incubated with primary antibodies
717 overnight at 4°C. Following three washes with PBS/0.1% Tween 20, membranes were
718 incubated with the appropriate HRP-conjugated secondary antibody at room temperature for 1h.
719 Signals were detected using Clarity ECL (Bio-Rad, #1705061) and SuperSignal West Femto
720 Maximum Sensitivity Substrate (Thermo Fisher, 34094) according to manufacturer's
721 instructions. Antibodies used: for immunoprecipitation, rabbit anti-GFP and for western blot,
722 rabbit anti-GFP (1:500, Invitrogen, #a11122), mouse anti-Myc (1:1000, DSHB, #9E10-C),

723 mouse anti-HA (1:1000, Biolegend, 901502), mouse anti-FLAG (1:1000, Sigma, F1804-50ug),
724 mouse anti-beta-tubulin (1:1000, DSHB, #E7) and HRP goat anti-mouse (1:10,000, Jackson
725 Immunoresearch, #115-035-146).

726 **Immunostaining**

727 Transiently transfected COS-7 cells were washed once with ice-cold PBS, fixed for 15 min in
728 4% paraformaldehyde at room temperature, permeabilized with 0.1% Triton X-100 in PBS (PBT)
729 for 10 min and then blocked in PBT + 5% NGS (normal goat serum) for 30 min at room
730 temperature. Cells were then incubated with primary antibodies diluted in PBT + 5% NGS
731 overnight at 4°C. After three washes in PBT, secondary antibodies diluted in PBT + 5% NGS
732 were added and incubated for 1h at room temperature. After secondary antibodies, cells were
733 washed three times in PBS and coverslips were mounted in Aquamount. The following
734 antibodies were used: Rabbit anti-Myc (1:500, Sigma, C3956-2MG), mouse anti-HA (1:500,
735 BioLegend # 901502), Alexa488 Goat anti-mouse (1:500, Invitrogen, #A11029), and Cy3 goat
736 anti-rabbit (1:500, Jackson Immunoresearch, 111-165-003).

737 Dechorionated, formaldehyde-fixed *Drosophila* embryos were fluorescently stained using
738 standard methods. The following antibodies were used: rabbit anti-GFP (1:250, Invitrogen,
739 #a11122), mouse anti-HA (1:500, BioLegend,#901502), rabbit anti-myc (1:500, Sigma, C3956-
740 2MG), chick anti-beta gal (1:500, Abcam, #ab9361),, mouse anti-Robo (1:50, DSHB, #13C9),
741 mouse anti BP102 (1:50, DHSB, BP102), Alexa647 goat anti-HRP (1:500, Jackson
742 Immunoresearch, #123-605-021), Alexa488 goat anti-rabbit (1:500, Invitrogen, #A11034),
743 Alexa488 goat anti-mouse (1:500, Invitrogen, #A11029), Alexa488 goat anti-chick (1:500,
744 Invitrogen, #A11039), Cy3 goat anti-mouse (1:500, Jackson Immunoresearch, #115-165-003),
745 Cy3 goat anti-Chick (1:500, Abcam, #ab97145), Cy3 goat anti-rabbit (1:500, Jackson
746 Immunoresearch, 111-165-003) and 647 goat anti-HRP (1:1,000, Jackson Immunoresearch,
747 #123-605-021). Embryos were filleted and mounted in 70% glycerol/1xPBS. Surface staining of

748 endogenous Robo in *Drosophila* embryos was carried out as previously described (Bashaw,
749 2010). Briefly, embryos were dissected live, blocked with in 5% normal goat serum (NGS) in
750 PBS for 15 min at 4°C and stained with mouse anti-Robo (1:50, DSHB, #13C9) in PBS for 30
751 min at 4°C. Following washes with PBS, embryos were fixed in 4% paraformaldehyde (Electron
752 Microscopy Services, #15710) for 15 min at 4°C. Following washes with PBS, fixed embryos
753 were then permeabilized with 0.1% Triton X-100 in PBS (PBT) for 10 min and stained with rabbit
754 anti-myc (1:500, Sigma, C3956-2MG) and 647 goat anti-HRP (1:1,000, Jackson
755 Immunoresearch, #123-605-021) in 5% NGS in PBT for one hour at room temperature.
756 Following washes with PBT, secondary antibody consisting of Alexa488 goat anti-mouse (1:500,
757 Invitrogen, #A11029) and Cy3 goat anti-rabbit (1:500, Jackson Immunoresearch, 111-165-003)
758 diluted in 5% NGS in PBT was added and incubated for 1 h at room temperature. Embryos were
759 then washed with PBT and mounted in 70% glycerol in PBS.

760 Fixed coverslips of COS-7 cells and samples of *Drosophila* embryo nerve cords were
761 imaged using a spinning disk confocal system (Perkin Elmer) built on a Nikon Ti-U inverted
762 microscope using a Nikon 40X or60X objective with Volocity imaging software. Images were
763 processed using NIH ImageJ software.

764 **Quantification and Statistical Analysis**

765 For analysis of *Drosophila* nerve cord phenotypes, image analysis was conducted blind to the
766 genotype. Data are presented as mean values ± 95% confidence interval. For statistical
767 analysis, comparisons were made between two groups using the Student's *t*-test. For multiple
768 comparisons, significance was assessed using one-way ANOVA with Tukey's *post hoc* tests.
769 Differences were considered significant when $p < 0.05$.

770 For quantification of biochemical data, blots were imaged with (what's the name of the
771 instrument) and quantification was performed using the densitometry function on ImageJ.

772 Comm, Robo, and Nedd4 levels in S2R+ cells or fly lysates are normalized to tubulin. For
773 immunoprecipitation experiments, ubiquitinated Robo was normalized to IGG, lysate Robo, and
774 tubulin. Nedd4 complex incorporation was normalized to immunoprecipitated Robo and lysate
775 Nedd4. Comparisons between two groups were made using Student's T test, and comparisons
776 between multiple groups were made using one-way ANOVA with Tukey's post-hoc test.
777 Differences were considered significant when $p < 0.05$.

778 For quantification of intracellular localization in COS-7 cells, images of seven cell fields
779 per condition were taken at random locations on the coverslip. Cells with overly bright staining,
780 in which we were unable to un-ambiguously observe intracellular localization, were excluded
781 from analysis. Only cells double positive for both HA and Myc were scored. Cells were scored
782 blind to condition. Distribution of exclusively punctate vs diffuse localization was compared
783 between groups using Chi Square.

784 For quantitation of Robo and Comm Levels in the nerve cord, in Drosophila embryos,
785 images were first batch processed using a macro in image J that set the channels of all images
786 to common thresholds. These processed images were then analyzed in CellProfiler. A common
787 thresholding algorithm was used on smoothened images of the HRP channel to create masks
788 for the nerve cord and axons. To quantify Robo, total Robo/488 intensity was measured within
789 the axon mask and divided by area of the mask. To quantify Comm, total Myc/Cy3 intensity was
790 calculated within the nerve cord mask and divided by area of the mask. Data are presented as
791 mean values ± 95% confidence interval. For statistical analysis, comparisons were made
792 between two groups using the Student's *t*-test, and between multiple groups using ANOVA with
793 Tukey's post-hoc test. Differences were considered significant when $p < 0.05$.

794 For quantification of cell body and axonal Comm localization, images were first batch
795 processed using a macro in image J that set the channels of all images to common thresholds.
796 These processed images were then analyzed in CellProfiler. A common smoothing algorithm

797 was applied to all images in the 488 channel (showing GFP-labelled apterous neurons). On this
798 smoothened image, both axons and cell bodies were automatically identified using an algorithm
799 that detects objects based on thresholding and size. This set of objects was then manually
800 edited to remove objects detected outside the appropriate area (posterior 8 segments of the
801 nerve cord). Using the original un-smoothened image in the 488 channel as a guide, objects
802 representing cell bodies were selected manually to generate a “cell body” mask. An “axon”
803 mask was generated by subtracting the manually-selected cell bodies from the total object set.
804 To quantify Comm expression in either cell bodies or axons, Cy3 fluorescence was measured
805 within the appropriate mask and divided by the area of those mask. The ratio of axonal Comm
806 to cell body Comm was then calculated. Comparisons between groups were made using one-
807 way ANOVA with Tukey’s Post-hoc test and data are represented as mean values +/- 95%
808 confidence intervals. Differences were considered significant when $p<0.05$.

809 For quantification of colocalization of Comm variants and late endosomal markers in
810 apterous neurons, images were first batch processed using a macro in image J that set the
811 channels of all images to common thresholds. These processed images were then analyzed in
812 cell profiler. To generate masks of cell bodies, a common smoothing algorithm was applied to all
813 images in the 488 channel (for either Rab7 GFP or Lamp1 GFP), and cell bodies were identified
814 automatically via an algorithm that recognizes objects based on brightness threshold, size, and
815 round shape. To generate a mask for the total area of Comm expression, a common smoothing
816 algorithm was applied to all images in the Cy3 Channel (for Comm). Areas of Comm expression
817 within the nerve cord (cell bodies as well as axons if Comm had axonal expression) were
818 identified automatically via an algorithm that recognizes objects based on size and brightness
819 threshold. To eliminate objects detected outside the appropriate area (for example, areas of
820 Comm expression in motor neurons as opposed to the nerve cord, or in the anterior four body
821 segments) objects were then manually edited using the original un-smoothened image in the

822 Cy3 channel. The final edited set of objects was then used to generate a mask. To enhance
823 both endosomal marker and Comm puncta, an algorithm was applied in both the 488 and Cy3
824 channels. Using the area of these enhanced images (within either the cell body mask, or total
825 comm expression mask) Comm colocalization with late endosomal markers was measured
826 using Pearson's Coefficient. Comparisons between groups were made using one way ANOVA
827 with Tukey's post-hoc test. Data are presented as mean values +/- 95% confidence intervals.
828 Differences were considered significant when $P<0.05$.

829 **Data and Software Availability:**

830 Confocal stacks were collected using a spinning disk confocal system (Perkin Elmer) built on a
831 Nikon Ti-U inverted microscope with Volocity imaging software. Images were processed using
832 NIH ImageJ and Adobe Photoshop software. Image analysis was conducted using CellProfiler
833 4.2.5. All statistics and graphs were generated using GraphPad Prism 9.

834 **Author Contributions**

835 Kelly Sullivan: Investigation, Methodology, Data curation, Formal analysis, Writing – original
836 draft, Writing – review and editing. Greg J. Bashaw: Investigation, Writing – review and editing,
837 Funding acquisition, Supervision. The authors declare no competing interests.

838 **Acknowledgements**

839 We would like to acknowledge past and present members of the Bashaw lab for thoughtful
840 discussions and comments on this manuscript. We especially thank Dr. Madhavi Gorla for
841 guidance on cell and biochemical assays, Dr. Yixin Zang for guidance on the embryo live-
842 dissection experiments and Dr. Camila Barrios Camacho for help with Cell Profiler analysis. The
843 *smurf 15C* fly line were a kind gift from Dr. Haiwei Pi. This research was supported by NIH
844 grants 5T32GM007229-42 and F31NS115345-01 to KS, and NSF Grant IOS-1853719 and NIH
845 Grant R35 NS097340 to G.J.B

846 **References**

847 Anitha, A., Nakamura, K., Yamada, K., Suda, S., Thanseem, I., Tsujii, M., Iwayama, Y., Hattori, E., Toyota,
848 T., Miyachi, T.*, et al.* (2008). Genetic analyses of roundabout (ROBO) axon guidance receptors in autism.
849 Am J Med Genet B Neuropsychiatr Genet *147B*, 1019-1027.
850 Arbeille, E., and Bashaw, G.J. (2018). Brain Tumor promotes axon growth across the midline through
851 interactions with the microtubule stabilizing protein Apc2. PLoS Genet *14*, e1007314.
852 Bakkers, J., Camacho-Carvajal, M., Nowak, M., Kramer, C., Danger, B., and Hammerschmidt, M. (2005).
853 Destabilization of DeltaNp63alpha by Nedd4-mediated ubiquitination and Ubc9-mediated sumoylation,
854 and its implications on dorsoventral patterning of the zebrafish embryo. Cell Cycle *4*, 790-800.
855 Bashaw, G.J. (2010). Live dissection and surface labeling of proteins in Drosophila embryos. Cold Spring
856 Harb Protoc *2010*, pdb prot5504.
857 Bosley, T.M., Salih, M.A., Jen, J.C., Lin, D.D., Oystreck, D., Abu-Amero, K.K., MacDonald, D.B., al Zayed, Z.,
858 al Dhalaan, H., Kansu, T.*, et al.* (2005). Neurologic features of horizontal gaze palsy and progressive
859 scoliosis with mutations in ROBO3. Neurology *64*, 1196-1203.
860 Brose, K., Bland, K.S., Wang, K.H., Arnott, D., Henzel, W., Goodman, C.S., Tessier-Lavigne, M., and Kidd,
861 T. (1999). Slit proteins bind Robo receptors and have an evolutionarily conserved role in repulsive axon
862 guidance. Cell *96*, 795-806.
863 Chance, R.K., and Bashaw, G.J. (2015). Slit-Dependent Endocytic Trafficking of the Robo Receptor Is
864 Required for Son of Sevenless Recruitment and Midline Axon Repulsion. PLoS Genet *11*, e1005402.
865 Charron, F., Stein, E., Jeong, J., McMahon, A.P., and Tessier-Lavigne, M. (2003). The Morphogen Sonic
866 Hedgehog Is an Axonal Chemoattractant that Collaborates with Netrin-1 in Midline Axon Guidance. Cell
867 *113*, 11-23.
868 Depienne, C., Cincotta, M., Billot, S., Bouteiller, D., Groppa, S., Brochard, V., Flamand, C., Hubsch, C.,
869 Meunier, S., Giovannelli, F.*, et al.* (2011). A novel DCC mutation and genetic heterogeneity in congenital
870 mirror movements. Neurology *76*, 260-264.
871 Engle, E.C. (2010). Human genetic disorders of axon guidance. Cold Spring Harb Perspect Biol *2*,
872 a001784.
873 Evans, T.A., and Bashaw, G.J. (2010). Axon guidance at the midline: of mice and flies. Curr Opin
874 Neurobiol *20*, 79-85.
875 Evans, T.A., Santiago, C., Arbeille, E., and Bashaw, G.J. (2015). Robo2 acts in trans to inhibit Slit-Robo1
876 repulsion in pre-crossing commissural axons. Elife *4*, e08407.
877 Foot, N.J., Dalton, H.E., Shearwin-Whyatt, L.M., Dorstyn, L., Tan, S.S., Yang, B., and Kumar, S. (2008).
878 Regulation of the divalent metal ion transporter DMT1 and iron homeostasis by a ubiquitin-dependent
879 mechanism involving Ndfips and WWP2. Blood *112*, 4268-4275.
880 Garbe, D.S., O'Donnell, M., and Bashaw, G.J. (2007). Cytoplasmic domain requirements for Frazzled-
881 mediated attractive axon turning at the Drosophila midline. Development *134*, 4325-4334.
882 Gilestro, G.F. (2008). Redundant mechanisms for regulation of midline crossing in Drosophila. PLoS One
883 *3*, e3798.
884 Gorla, M., and Bashaw, G.J. (2020). Molecular mechanisms regulating axon responsiveness at the
885 midline. Dev Biol *466*, 12-21.
886 Gorla, M., Chaudhari, K., Hale, M., Potter, C., and Bashaw, G.J. (2022). A Nedd4 E3 Ubiquitin Ligase
887 Pathway Inhibits Robo1 Repulsion and Promotes Commissural Axon Guidance across the Midline. J
888 Neurosci *42*, 7547-7561.
889 Gorla, M., Santiago, C., Chaudhari, K., Layman, A.A.K., Oliver, P.M., and Bashaw, G.J. (2019). Ndfip
890 Proteins Target Robo Receptors for Degradation and Allow Commissural Axons to Cross the Midline in
891 the Developing Spinal Cord. Cell Rep *26*, 3298-3312 e3294.

892 Hernandez-Fleming, M., Rohrbach, E.W., and Bashaw, G.J. (2017). Sema-1a Reverse Signaling Promotes
893 Midline Crossing in Response to Secreted Semaphorins. Cell Rep *18*, 174-184.
894 Howitt, J., Putz, U., Lackovic, J., Doan, A., Dorstyn, L., Cheng, H., Yang, B., Chan-Ling, T., Silke, J., Kumar,
895 S.*, et al.* (2009). Divalent metal transporter 1 (DMT1) regulation by Ndfip1 prevents metal toxicity in
896 human neurons. Proc Natl Acad Sci U S A *106*, 15489-15494.
897 Ing, B., Shteiman-Kotler, A., Castelli, M., Henry, P., Pak, Y., Stewart, B., Boulianne, G.L., and Rotin, D.
898 (2007). Regulation of Commissureless by the ubiquitin ligase DNedd4 is required for neuromuscular
899 synaptogenesis in Drosophila melanogaster. Mol Cell Biol *27*, 481-496.
900 Ingham, R.J., Gish, G., and Pawson, T. (2004). The Nedd4 family of E3 ubiquitin ligases: functional
901 diversity within a common modular architecture. Oncogene *23*, 1972-1984.
902 Ishii, N., Wadsworth, W.G., Stern, B.D., Culotti, J.G., and Hedgecock, E.M. (1992). UNC-6, a laminin-
903 related protein, guides cell and pioneer axon migrations in C. elegans. Neuron *9*, 873-881.
904 Izzi, L., and Charron, F. (2011). Midline axon guidance and human genetic disorders. Clin Genet *80*, 226-
905 234.
906 Jamuar, S.S., Schmitz-Abe, K., D'Gama, A.M., Drottar, M., Chan, W.M., Peeva, M., Servattalab, S., Lam,
907 A.N., Delgado, M.R., Clegg, N.J.*, et al.* (2017). Biallelic mutations in human DCC cause developmental
908 split-brain syndrome. Nat Genet *49*, 606-612.
909 Justice, E.D., Barnum, S.J., and Kidd, T. (2017). The WAGR syndrome gene PRRG4 is a functional
910 homologue of the commissureless axon guidance gene. PLoS Genet *13*, e1006865.
911 Kanelis, V., Bruce, M.C., Skrynnikov, N.R., Rotin, D., and Forman-Kay, J.D. (2006). Structural determinants
912 for high-affinity binding in a Nedd4 WW3* domain-Comm PY motif complex. Structure *14*, 543-553.
913 Kanelis, V., Rotin, D., and Forman-Kay, J.D. (2001). Solution structure of a Nedd4 WW domain-ENaC
914 peptide complex. Nat Struct Biol *8*, 407-412.
915 Kang, Y., Guo, J., Yang, T., Li, W., and Zhang, S. (2015). Regulation of the human ether-a-go-go-related
916 gene (hERG) potassium channel by Nedd4 family interacting proteins (Ndfips). Biochem J *472*, 71-82.
917 Kasanov, J., Pirozzi, G., Uveges, A.J., and Kay, B.K. (2001). Characterizing Class I WW domains defines key
918 specificity determinants and generates mutant domains with novel specificities. Chem Biol *8*, 231-241.
919 Keleman, K., Rajagopalan, S., Cleppien, D., Teis, D., Paiha, K., Huber, L.A., Technau, G.M., and Dickson,
920 B.J. (2002). Comm Sorts Robo to Control Axon Guidance at the Drosophila Midline. Cell *110*, 415-427.
921 Keleman, K., Ribeiro, C., and Dickson, B.J. (2005). Comm function in commissural axon guidance: cell-
922 autonomous sorting of Robo in vivo. Nat Neurosci *8*, 156-163.
923 Kidd, T., Bland, K.S., and Goodman, C.S. (1999). Slit Is the Midline Repellent for the Robo Receptor in
924 Drosophila. Cell *96*, 785-794.
925 Kidd, T., Russell, C., Goodman, C.S., and Tear, G. (1998). Dosage-sensitive and complementary functions
926 of roundabout and commissureless control axon crossing of the CNS midline. Neuron *20*, 25-33.
927 Kinoshita-Kawada, M., Hasegawa, H., Hongu, T., Yanagi, S., Kanaho, Y., Masai, I., Mishima, T., Chen, X.,
928 Tsuboi, Y., Rao, Y.*, et al.* (2019). A crucial role for Arf6 in the response of commissural axons to Slit.
929 Development *146*.
930 Lin, C.M., Xu, J., Yang, W.T., Wang, C., Li, Y.C., Cheng, L.C., Zhang, L., and Hsu, J.C. (2017). Smurf
931 Downregulates Echinoid in the Amnioserosa To Regulate Drosophila Dorsal Closure. Genetics *206*, 985-
932 992.
933 Lohraseb, I., McCarthy, P., Secker, G., Marchant, C., Wu, J., Ali, N., Kumar, S., Daly, R.J., Harvey, N.L.,
934 Kawabe, H.*, et al.* (2022). Global ubiquitinome profiling identifies NEDD4 as a regulator of Profilin 1 and
935 actin remodelling in neural crest cells. Nat Commun *13*, 2018.
936 Mitchell, K.J., Doyle, J.L., Serafini, T., Kennedy, T.E., Tessier-Lavigne, M., Goodman, C.S., and Dickson, B.J.
937 (1996). Genetic analysis of Netrin genes in Drosophila: Netrins guide CNS commissural axons and
938 peripheral motor axons. Neuron *17*, 203-215.

939 Mund, T., and Pelham, H.R. (2010). Regulation of PTEN/Akt and MAP kinase signaling pathways by the
940 ubiquitin ligase activators Ndfip1 and Ndfip2. Proc Natl Acad Sci U S A *107*, 11429-11434.
941 Myat, A., Henry, P., McCabe, V., Flintoft, L., Rotin, D., and Tear, G. (2002). Drosophila Nedd4, a Ubiquitin
942 Ligase, Is Recruited by Commissureless to Control Cell Surface Levels of the Roundabout Receptor.
943 Neuron *35*, 447-459.
944 Nagarkar-Jaiswal, S., Lee, P.T., Campbell, M.E., Chen, K., Anguiano-Zarate, S., Gutierrez, M.C., Busby, T.,
945 Lin, W.W., He, Y., Schulze, K.L.*, et al.* (2015). A library of MiMICs allows tagging of genes and reversible,
946 spatial and temporal knockdown of proteins in Drosophila. Elife *4*.
947 Nawabi, H., and Castellani, V. (2011). Axonal commissures in the central nervous system: how to cross
948 the midline? Cell Mol Life Sci *68*, 2539-2553.
949 Paul, L.K., Brown, W.S., Adolphs, R., Tyszka, J.M., Richards, L.J., Mukherjee, P., and Sherr, E.H. (2007).
950 Agenesis of the corpus callosum: genetic, developmental and functional aspects of connectivity. Nat Rev
951 Neurosci *8*, 287-299.
952 Persaud, A., Alberts, P., Hayes, M., Guettler, S., Clarke, I., Sicheri, F., Dirks, P., Ciruna, B., and Rotin, D.
953 (2011). Nedd4-1 binds and ubiquitylates activated FGFR1 to control its endocytosis and function. EMBO J
954 *30*, 3259-3273.
955 Podos, S.D., Hanson, K.K., Wang, Y.C., and Ferguson, E.L. (2001). The DSmurf ubiquitin-protein ligase
956 restricts BMP signaling spatially and temporally during Drosophila embryogenesis. Dev Cell *1*, 567-578.
957 Roney, J.C., Cheng, X.T., and Sheng, Z.H. (2022). Neuronal endolysosomal transport and lysosomal
958 functionality in maintaining axonostasis. J Cell Biol *221*.
959 Sabatier, C., Plump, A.S., Le, M., Brose, K., Tamada, A., Murakami, F., Lee, E.Y., and Tessier-Lavigne, M.
960 (2004). The divergent Robo family protein rig-1/Robo3 is a negative regulator of slit responsiveness
961 required for midline crossing by commissural axons. Cell *117*, 157-169.
962 Sakata, T., Sakaguchi, H., Tsuda, L., Higashitani, A., Aigaki, T., Matsuno, K., and Hayashi, S. (2004).
963 Drosophila Nedd4 regulates endocytosis of notch and suppresses its ligand-independent activation. Curr
964 Biol *14*, 2228-2236.
965 Serafini, T., Colamarino, S.A., Leonardo, E.D., Wang, H., Beddington, R., Skarnes, W.C., and Tessier-
966 Lavigne, M. (1996). Netrin-1 is required for commissural axon guidance in the developing vertebrate
967 nervous system. Cell *87*, 1001-1014.
968 Serafini, T., Kennedy, T.E., Galko, M.J., Mirzayan, C., Jessell, T.M., and Tessier-Lavigne, M. (1994). The
969 netrins define a family of axon outgrowth-promoting proteins homologous to C. elegans UNC-6. Cell *78*,
970 409-424.
971 Spitzweck, B., Brankatschk, M., and Dickson, B.J. (2010). Distinct protein domains and expression
972 patterns confer divergent axon guidance functions for Drosophila Robo receptors. Cell *140*, 409-420.
973 Srour, M., Riviere, J.B., Pham, J.M., Dube, M.P., Girard, S., Morin, S., Dion, P.A., Asselin, G., Rochefort, D.,
974 Hince, P.*, et al.* (2010). Mutations in DCC cause congenital mirror movements. Science *328*, 592.
975 Suda, S., Iwata, K., Shimmura, C., Kameno, Y., Anitha, A., Thanseem, I., Nakamura, K., Matsuzaki, H.,
976 Tsuchiya, K.J., Sugihara, G.*, et al.* (2011). Decreased expression of axon-guidance receptors in the
977 anterior cingulate cortex in autism. Mol Autism *2*, 14.
978 Sullivan, K.G., and Bashaw, G.J. (2023). Intracellular Trafficking Mechanisms that Regulate Repulsive
979 Axon Guidance. Neuroscience *508*, 123-136.
980 Tear, G., Harris, R., Sutaria, S., Kilomanski, K., Goodman, C.S., and Seeger, M.A. (1996). commissureless
981 controls growth cone guidance across the CNS midline in Drosophila and encodes a novel membrane
982 protein. Neuron *16*, 501-514.
983 Trimpert, C., Wesche, D., de Groot, T., Pimentel Rodriguez, M.M., Wong, V., van den Berg, D.T.M.,
984 Cheval, L., Ariza, C.A., Doucet, A., Stagljar, I.*, et al.* (2017). NDFIP allows NEDD4/NEDD4L-induced AQP2
985 ubiquitination and degradation. PLoS One *12*, e0183774.

986 Wolf, B., Seeger, M.A., and Chiba, A. (1998). Commissureless endocytosis is correlated with initiation of
987 neuromuscular synaptogenesis. Development (Cambridge, England) *125*, 3853-3863.
988 Xia, L., Jia, S., Huang, S., Wang, H., Zhu, Y., Mu, Y., Kan, L., Zheng, W., Wu, D., Li, X.*, et al.* (2010). The
989 Fused/Smurf complex controls the fate of Drosophila germline stem cells by generating a gradient BMP
990 response. Cell *143*, 978-990.
991 Yuasa-Kawada, J., Kinoshita-Kawada, M., Wu, G., Rao, Y., and Wu, J.Y. (2009). Midline crossing and Slit
992 responsiveness of commissural axons require USP33. Nat Neurosci *12*, 1087-1089.
993 Zhang, Y., Ding, Y., Chen, Y.G., and Tao, Q. (2014). NEDD4L regulates convergent extension movements
994 in Xenopus embryos via Disheveled-mediated non-canonical Wnt signaling. Dev Biol *392*, 15-25.
995 Zou, Y., Stoeckli, E., Chen, H., and Tessier-Lavigne, M. (2000). Squeezing axons out of the gray matter: a
996 role for slit and semaphorin proteins from midline and ventral spinal cord. Cell *102*, 363-375.

997
998

999 **Figures and Legends**

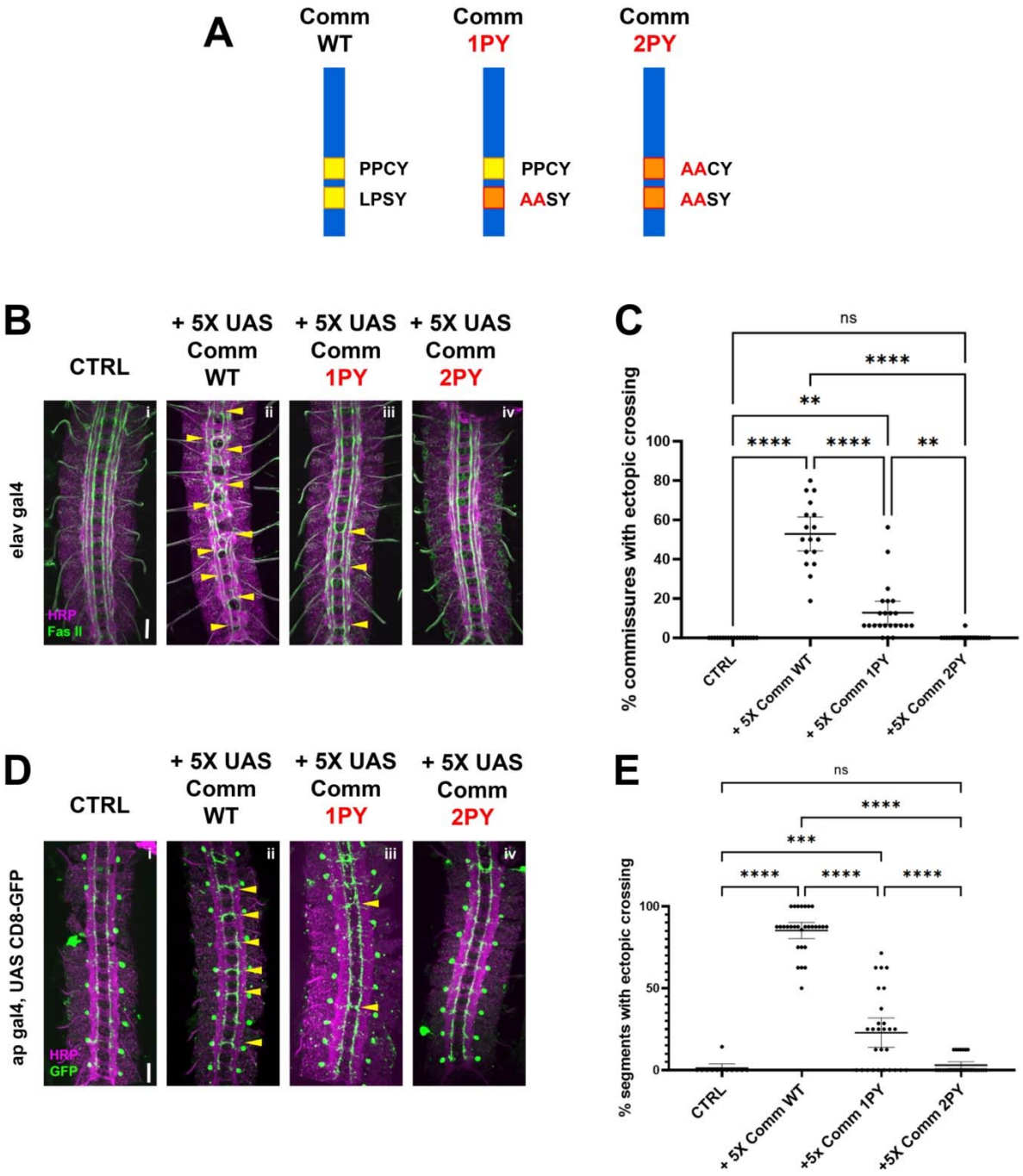

1000

1001 **<u>Figure 1. PY motifs are required for Comm to promote midline crossing</u>**

1002 A) Comm variants used in this study including WT, and mutant forms in which the LPSY (1PY)

1003 or both the LPSY and PPCY (2PY) motifs are disrupted. B-C) PY motifs are necessary for

1004 Comm to cause ectopic crossing in the ipsilateral FasII neuron population when driven pan-
1005 neuronally. B) Micrographs of stage 16-17 nerve cords stained with HRP (pan-neuronal marker,
1006 magenta) and FasII (green) expressing no Comm (i), Comm WT (ii), Comm 1PY (iii), and Comm
1007 2PY (iv) under the elav gal4 driver. C) Quantification of ectopic FasII crossing in stage 16-17
1008 embryos expressing wild type and PY-mutant Comm variants. Groups were compared using
1009 ANOVA with Tukey's post-hoc test, and error bars represent mean with 95% confidence
1010 interval. D-E) PY motifs are required for Comm to cell-autonomously promote ectopic midline
1011 crossing when driven in apterous neurons. D) Micrographs of stage 16-17 nerve cords stained
1012 with HRP (magenta) and GFP (green), expressing GFP and no Comm (i), Comm WT (ii), Comm
1013 1PY (iii), and Comm 2PY (iv) under the ap gal4 driver. E) Quantification of ectopic apterous
1014 neuron crossing in stage 16-17 embryos expressing wild type and PY-mutant Comm variants.
1015 Groups were compared using ANOVA with Tukey's post-hoc test, and error bars represent
1016 mean with 95% confidence interval. For all graphs, each data point represents one embryo. **
1017 ($p<0.01$) **** ($p<0.0001$). Scale bars represent 20μM.
1018
1019

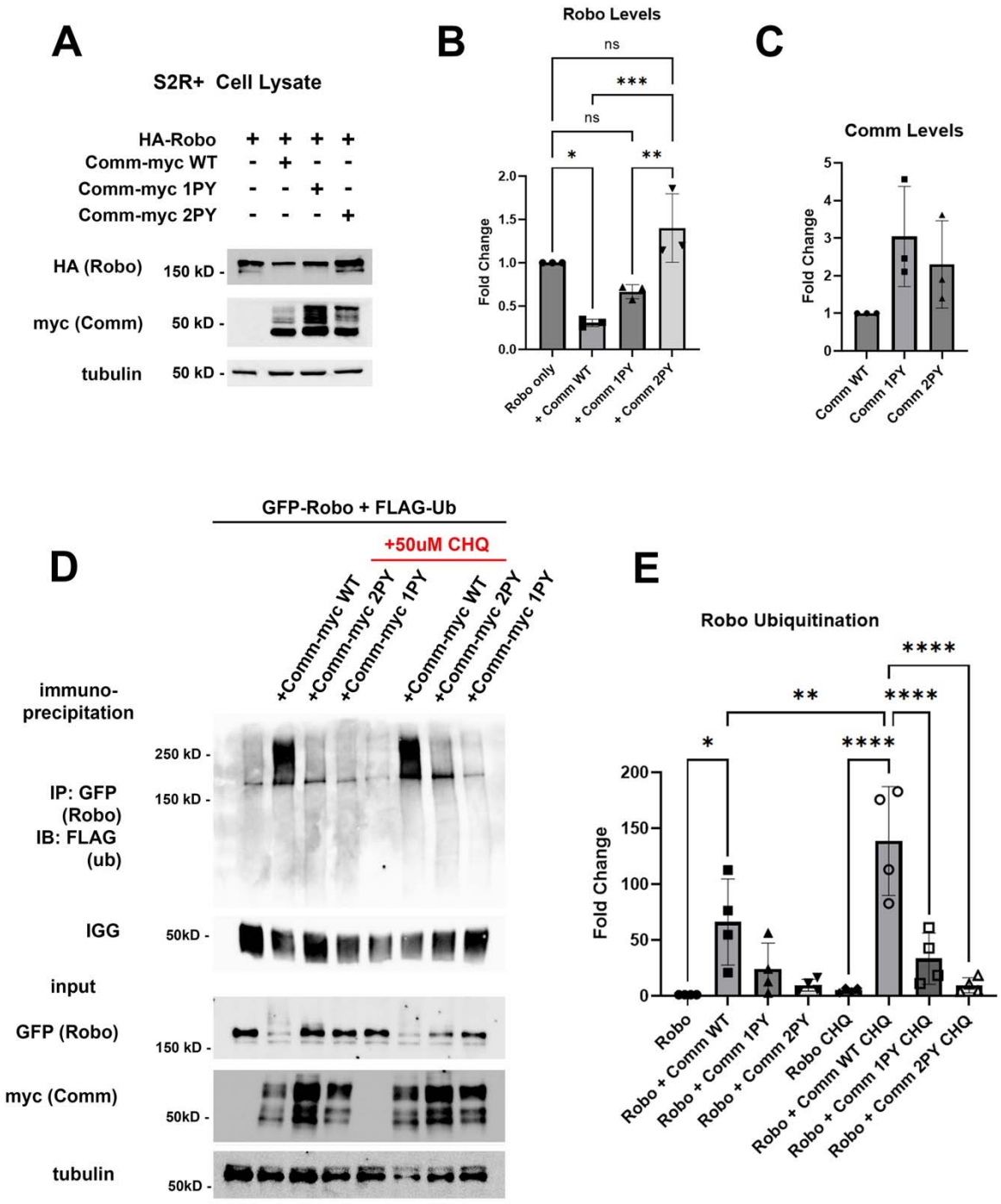

Figure 2. PY motifs are required for Comm to downregulate Robo1 protein levels *in vitro*. A-C) Loss of PY motifs inhibits Robo1 degradation facilitated by Comm and increases Comm stability. A) Western blot of S2R+ cells transfected with HA-Robo1 and Comm-Myc WT, 1PY, or 2PY. B) Fold change in Robo1 levels relative to the “Robo1 alone” condition. Protein levels were

1025 calculated via densitometry and normalized to tubulin. C) Fold change in Comm levels relative
1026 to the “WT Comm” condition. Protein levels were calculated via densitometry and normalized to
1027 tubulin. For B and C, groups were compared using ANOVA with Tukey’s post hoc test. Error
1028 bars represent mean +/- SD. Each data point represents values calculated from a single
1029 experiment. * ($p<0.05$), ** ($p<0.01$), *** ($p<0.001$). D-E) Comm requires PY motifs to facilitate
1030 Robo1 ubiquitination and degradation in the lysosome. D) Immunoprecipitation of ubiquitinated
1031 Robo1 in control or chloroquine-treated S2R+ cells transfected with FLAG-Ubiquitin and HA-
1032 Robo1 alone, or HA-Robo1 and WT, 1PY, or 2PY Comm-myc variants. Cells were incubated
1033 with Chloroquine for 2 hrs. E) Fold change of ubiquitinated Robo1 levels relative to the “Robo1
1034 only” condition. Ubiquitinated Robo1 levels were measured by quantifying immunoprecipitated
1035 FLAG blotting via densitometry and normalizing to IGG, lysate Robo1, and tubulin. For B and C,
1036 groups were compared using ANOVA with Tukey’s post hoc test. Error bars represent mean +/-
1037 SD. Each data point represents values calculated from a single experiment * ($p<0.05$), **
1038 ($p<0.01$), **** ($p<0.0001$).
1039

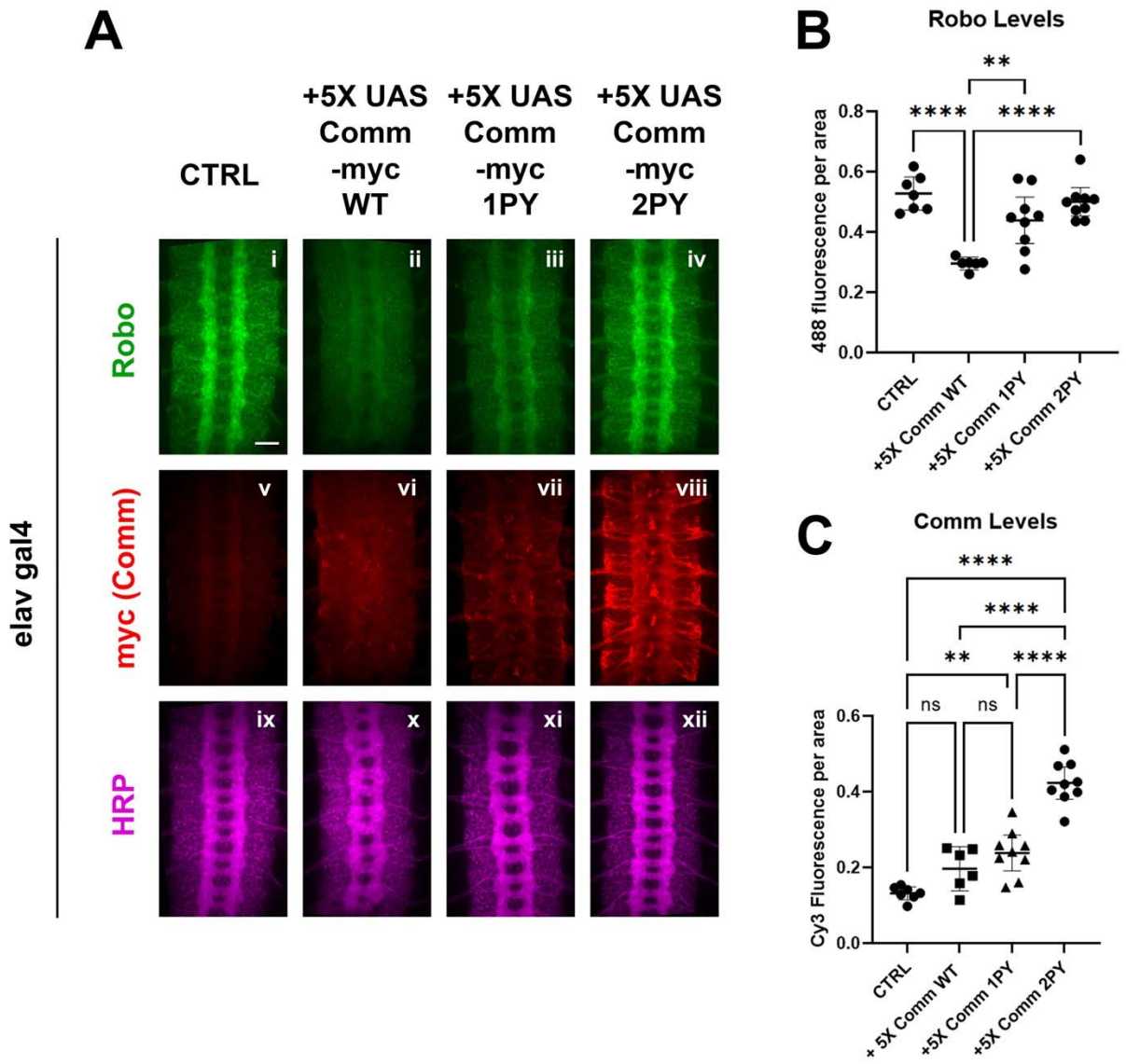

Figure 3: PY motifs are necessary for Comm to downregulate Robo protein levels *in vivo*. A) Stage 15-16 embryos expressing no Comm or 5X UAS Comm-myc variants under the pan neuronal elav gal4 driver. Embryos are stained for endogenous Robo1 (i-iv) , Myc (v-viii), and pan-neuronal marker HRP (ix-xii). Scale bar represents 20μM. B) Quantification of endogenous Robo1 levels in stage 15-16 embryos expressing Comm variants under elav gal4 driver. Robo1 levels were measured by creating a mask of the axonal scaffold, measuring 488 fluorescence within the scaffold, and dividing by scaffold area. C) Quantification of Comm levels in stage 15-16 embryos expressing Comm variants under the *elavGal4* driver. Comm levels were measured

1049 by creating a mask of the whole nerve cord, measuring Cy3 fluorescence within the nerve cord,
1050 and dividing by nerve cord area. For B and C, groups were compared using ANOVA with
1051 Tukey's post-hoc test. ** $p<0.01$ **** $p<0.0001$. Error bars represent 95% confidence intervals
1052 around the mean. Each data point represents one embryo.
1053

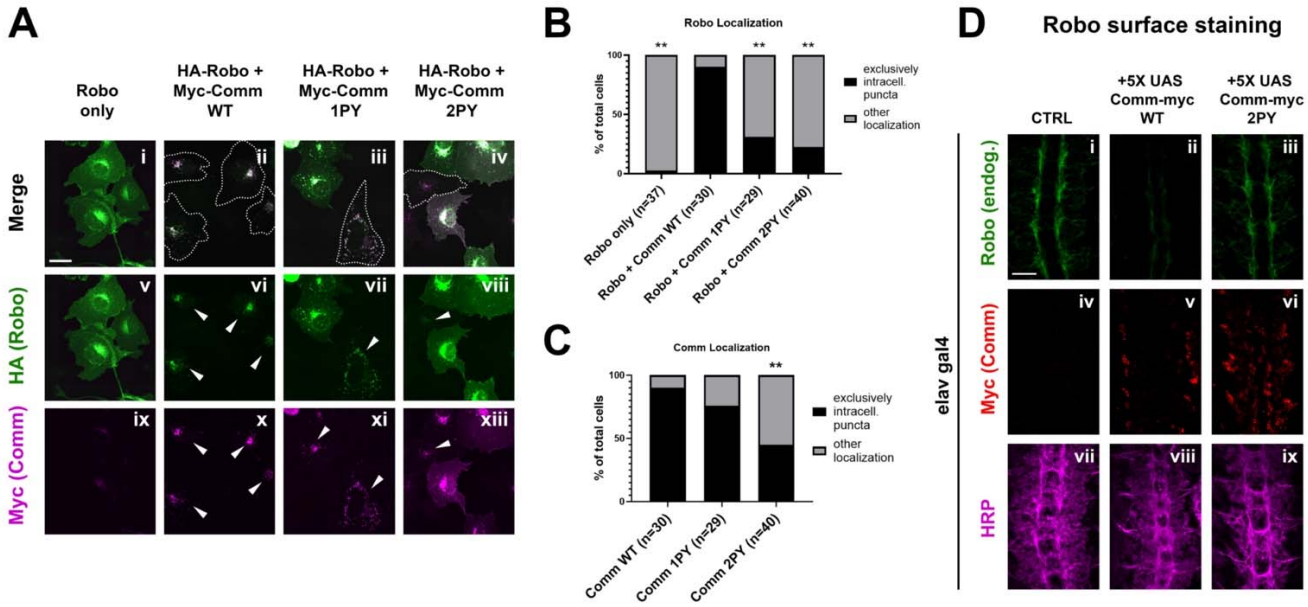

Figure 4: PY motifs are necessary for Comm to effectively traffic Robo1.

A) COS-7 cells transfected with HA-Robo1 and Myc-Comm variants. Cells in which Comm and Robo1 are exclusively in puncta are outlined with dotted lines in merged images and labelled with arrowheads in images of individual color channels. Scale bar represents 15μM. B) Quantification of cells expressing Robo1 exclusively in intracellular puncta or in diffuse localization throughout the cell. N represents the number of individual cells counted, which were taken from seven images of cell fields chosen at random locations on the microscope slide. Distribution of exclusively punctate vs diffuse Robo1 localization in Comm-transfected conditions was compared to the Robo1 alone condition via Chi Square (** $p<0.01$). C) Quantification of cells expressing Comm exclusively in intracellular puncta or in diffuse localization throughout the cell. N represents the number of individual cells counted, which were taken from seven images of cell fields chosen at random locations on the microscope slide. Distribution of exclusively punctate vs diffuse Comm localization in comm mutant conditions was compared to the WT Comm condition via Chi Square (** $p<0.01$). In both B and C, only cells expressing both Comm and Robo1 were counted. D) Surface expression of Robo in nerve cords

1071 of stage 14-15 embryos. Embryos were live-dissected, left unpermeabilized, and stained with an
1072 antibody against endogenous Robo1 at 4°C. After Robo1 staining, embryos were permeabilized
1073 and stained with HRP and Myc. Scale bar represents 20μM.
1074

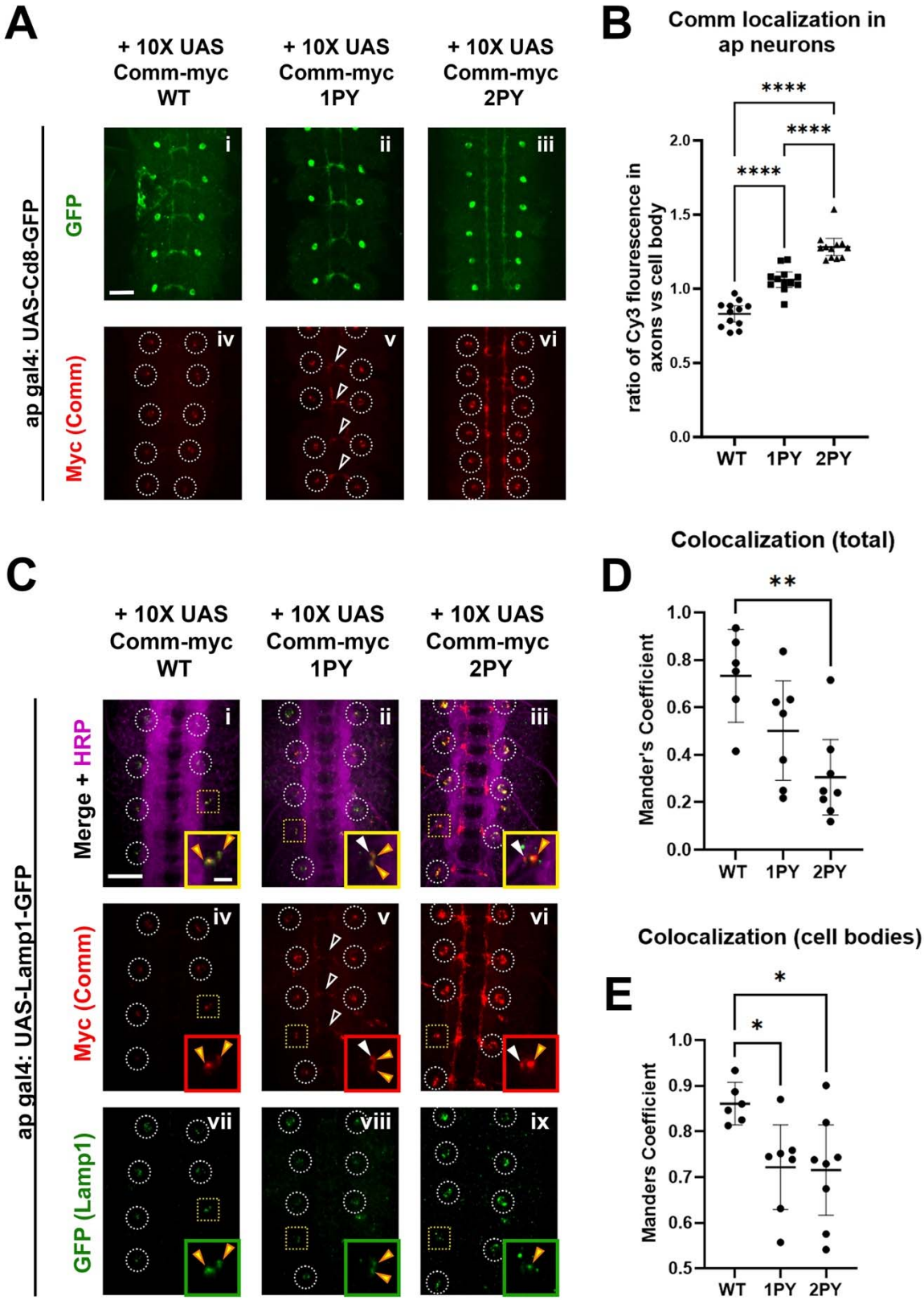
A
+ 10X UAS Comm-myc WT
+ 10X UAS Comm-myc 1PY
+ 10X UAS Comm-myc 2PY
ap gal4: UAS-Cd8-GFP
GFP
Myc (Comm)
i
ii
iii
iv
v
vi
B
Comm localization in ap neurons
ratio of Cy3 flourescence in axons vs cell body
****
****
****
WT
1PY
2PY
C
+ 10X UAS Comm-myc WT
+ 10X UAS Comm-myc 1PY
+ 10X UAS Comm-myc 2PY
ap gal4: UAS-Lamp1-GFP
Merge + HRP
Myc (Comm)
GFP (Lamp1)
i
ii
iii
iv
v
vi
vii
viii
ix
D
Colocalization (total)
Mander's Coefficient
**
WT
1PY
2PY
E
Colocalization (cell bodies)
Manders Coefficient
*
*
WT
1PY
2PY

1075

1076 **Figure 5: Comm requires intact PY motifs to localize appropriately *in vivo*.**

1077 A) Micrographs of stage 16-17 embryos expressing CD8-GFP and WT or PY-mutant Comm-
1078 myc variants under the apgal4 driver. Embryos are stained with GFP to visualize apterous
1079 neurons, Myc (Comm), and HRP (pan neuronal marker). Cell bodies are circled in panels
1080 showing Myc staining (iv-vi). In v, axonal Comm expression is indicated with arrowheads. Scale
1081 bar represents 20μM. B) Quantification of the ratio of axonal Comm to cell soma Comm in stage
1082 17 embryos expressing WT and PY-mutant Comm variants in apterous neurons. Axonal and
1083 cell soma comm were measured within masks created of these two features, derived from
1084 images of apterous neurons in the GFP channel. Axon/cell soma ratios were compared via
1085 ANOVA with Tukey's post-hoc test (**** $p<0.0001$). Error bars represent 95% confidence
1086 intervals around the mean. Each data point represents a single embryo. C) Stage 15 embryos
1087 expressing Lamp1-GFP and WT or PY-mutant Comm myc variants under the *apGal4* driver.
1088 Embryos are stained with GFP (Lamp1), Myc (Comm), and HRP (pan neuronal marker). Cell
1089 bodies are outlined with white circles except those that are enlarged in inset images, which are
1090 outlined with yellow squares. Within inset images, Comm/Lamp1 co-positive puncta are
1091 indicated with yellow arrowheads and puncta containing Comm alone are indicated with white
1092 arrowheads. Scale bar represents 20μM in the large image and 5μM in the inset image. D) Total
1093 colocalization of Comm and Lamp1. The proportion of areas of Comm expression that were also
1094 positive for Lamp1 was calculated via pearson's coefficient within a mask created of the area of
1095 Comm expression using smoothened images from the Comm channel. E) Colocalization of
1096 Comm and Lamp1 within cell bodies. The proportion of areas of Comm expression that were
1097 also positive for Lamp1 was calculated via Pearson's coefficient within a mask created of cell
1098 bodies using smoothened images from the Lamp1 channel. For D and E, colocalization across
1099 conditions was compared via ANOVA with Tukey's post hoc test (* $p<0.05$, ** $p<0.01$). Error
1100 bars represent 95% confidence intervals around the mean. Each data point represents one
1101 embryo.

1102

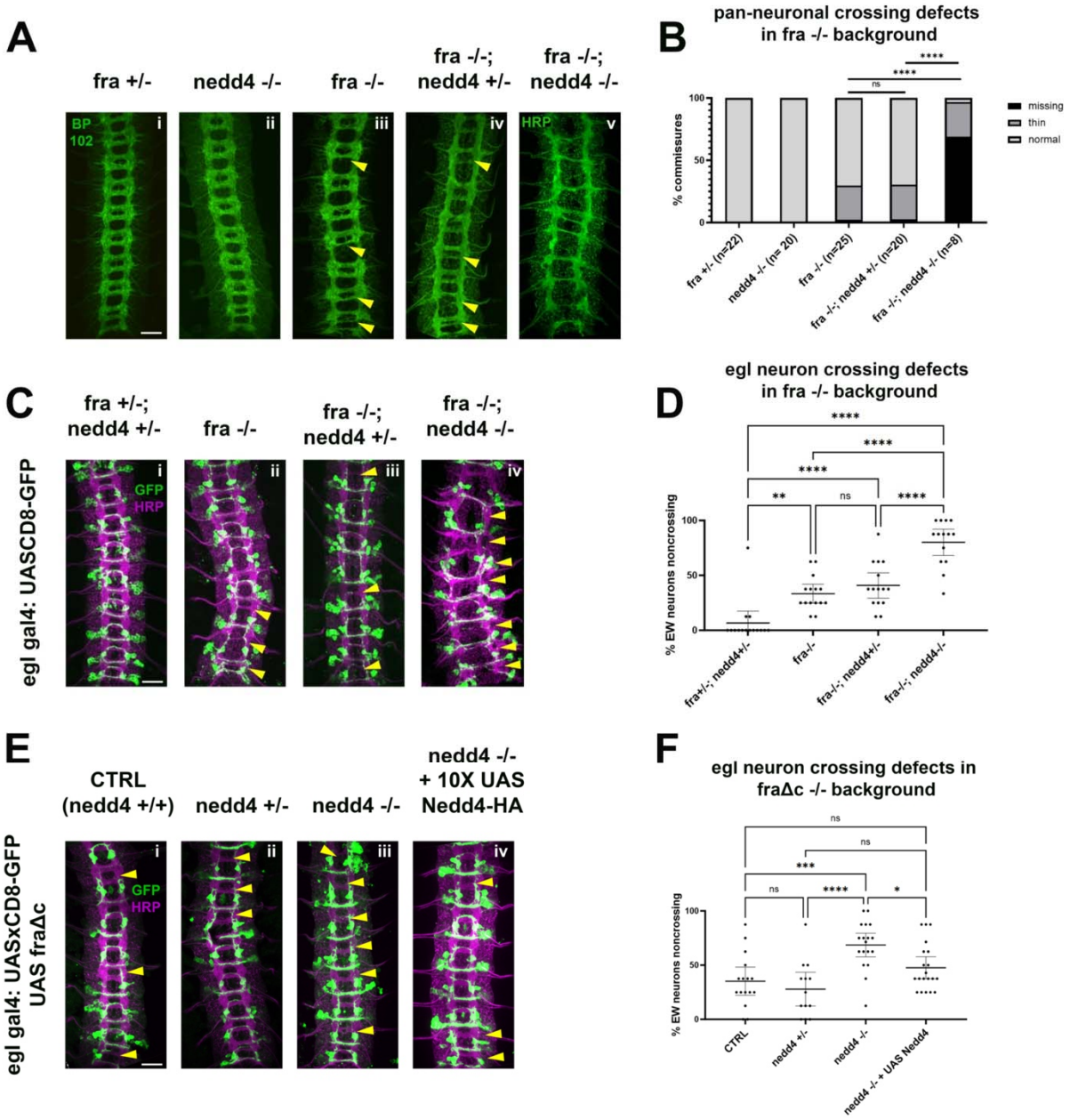

1103

1104 **<u>Figure 6: Nedd4 is required for midline crossing in vivo.</u>** A-B) Loss of *nedd4* enhances pan

1105 neuronal crossing defects in a *fra-/-* background. A) Stage 15-16 embryos with various

1106 combinations of *wild-type* and null *fra* and *nedd4* alleles, stained with pan-neuronal markers

1107 BP102 (i-iv) and HRP (v). Commissures with crossing defects (either thin or completely missing)

1108 are indicated with yellow arrowheads. B) Quantification of crossing defects in embryos within

1109 the genotypes indicated in A. Percentage of total crossing defects was compared across groups
1110 using ANOVA (** $p<0.01$, **** $p<0.0001$). N represents number of individual embryos. C-D) Loss
1111 of *nedd4* enhances EW crossing defects in a *fra -/-* background. C) Stage 15-16 embryos with
1112 various combinations of wild-type and null *fra* and *nedd4* alleles, expressing GFP under the egl
1113 gal4 driver. Embryos are stained with pan-neuronal marker HRP, and GFP to visualize eg
1114 neurons. Commissures with EW crossing defects are indicated with arrowheads. D)
1115 Quantification of crossing defects in embryos within the genotypes indicated in (C). Percentage
1116 of crossing defects was compared across groups using ANOVA (** $p<0.01$, **** $p<0.0001$).
1117 Each data point represents an individual embryo and error bars represent 95% confidence
1118 intervals around the mean E-F) Loss of *nedd4* enhances EW crossing defects in the fraΔc
1119 background. E) Embryos with *nedd4* mutations and/or exogenous Nedd4 expression in the
1120 fraΔc background. F) Quantification of EW crossing defects for the genotypes shown in (E).
1121 Percentage of crossing defects was compared across groups using ANOVA (** $p<0.01$, ****
1122 $p<0.0001$). Each data point represents an individual embryo and error bars represent95%
1123 confidence intervals around the mean. All scale bars represent 20μM.
1124
1125

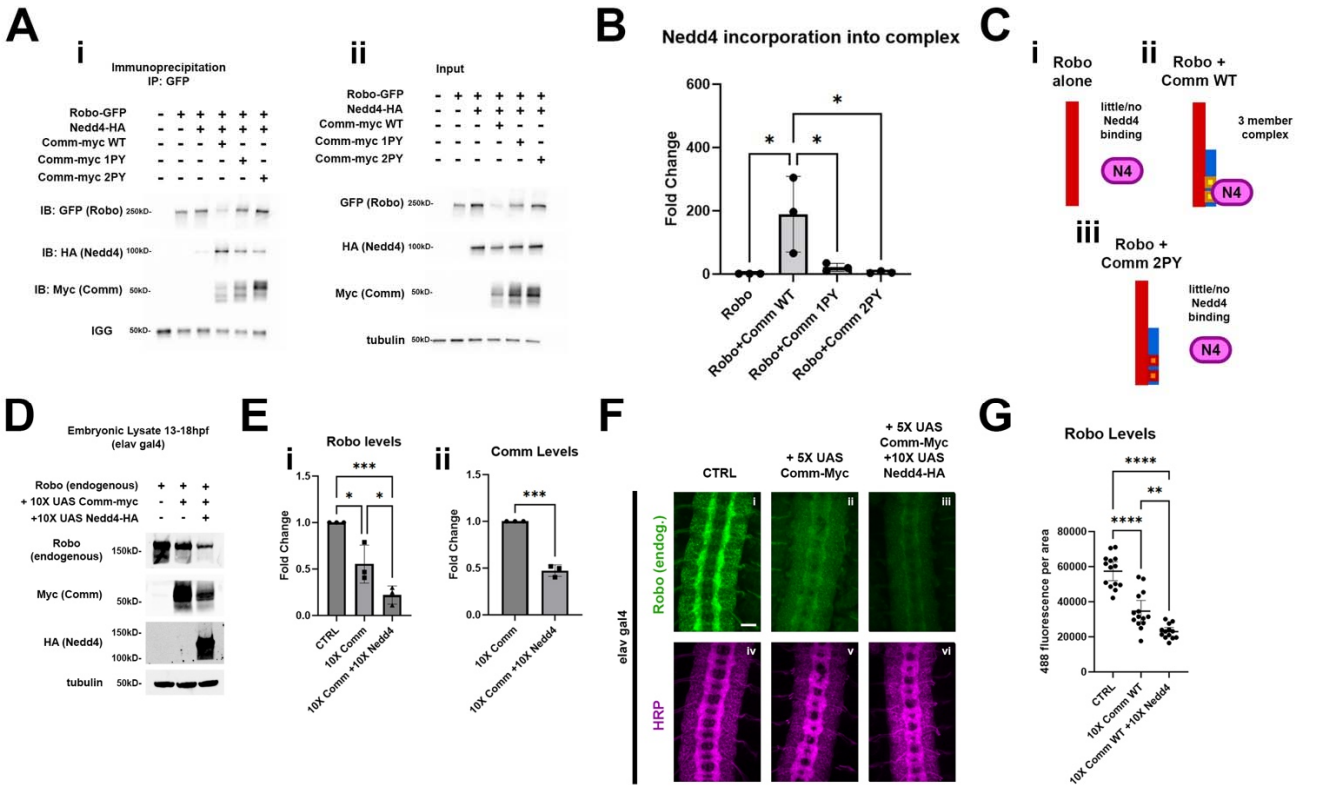

Figure 7: Nedd4 interacts genetically and biochemically with slit/Robo1 pathway.

A-C) Nedd4 is incorporated into a three-member complex with Robo1 and Comm. A) immunoprecipitation (i) and input (ii) of Robo1-GFP in S2R+ cells co-transfected with Nedd4-HA and WT, 1PY, or 2PY Comm-myc variants. B) Quantification of fold change in Nedd4 association with Robo1, relative to the Robo1 + Nedd4 condition, from the co-immunoprecipitation in (A). This was measured by quantifying immunoprecipitated Nedd4 via densitometry and normalizing to immunoprecipitated Robo1 and input Nedd4. Groups were compared using ANOVA with Tukey's post-hoc test. (* $p<0.05$) Error bars represent mean +/- one standard deviation. C) Schematic illustrating how Nedd4 relies on Comm PY motifs for recruitment into a ternary complex with Robo1 and Nedd4. D-G) Exogenous Nedd4 enhances degradation of Robo1 in the presence of WT Comm *in vivo*. D) Western blot of Lysates of 13-18hpf embryos expressing WT Comm-myc with or without Nedd4-HA under the elavGal4 driver. E) Quantification of Robo1 (i) and Comm (ii) levels from the blot in (D). Protein levels were

1140 measured via densitometry and normalized to tubulin. Protein levels were compared across
1141 conditions using ANOVA with Tukey's post-hoc test. (* $p<0.05$, *** $p<0.001$, **** $p<0.0001$) Error
1142 bars represent mean +/- one standard deviation. F) Nerve cords of stage 15-16 embryos
1143 expressing WT Comm-myc with or without Nedd4-HA under the elavGal4 driver. Embryos are
1144 stained with the pan neuronal marker HRP (magenta) and an antibody against endogenous
1145 Robo1 (green). Scale bar represents 20μM. G) Quantification of Robo1 levels from the
1146 conditions in (F). Robo1 levels were measured by creating a mask of the axonal scaffold,
1147 measuring 488 fluorescence within the scaffold, and dividing by scaffold area. Robo1 levels
1148 were compared across conditions using ANOVA with Tukey's post-hoc test. (** $p<0.01$, ****
1149 $p<0.0001$) Error bars represent 95% confidence intervals around the mean.
1150
1151

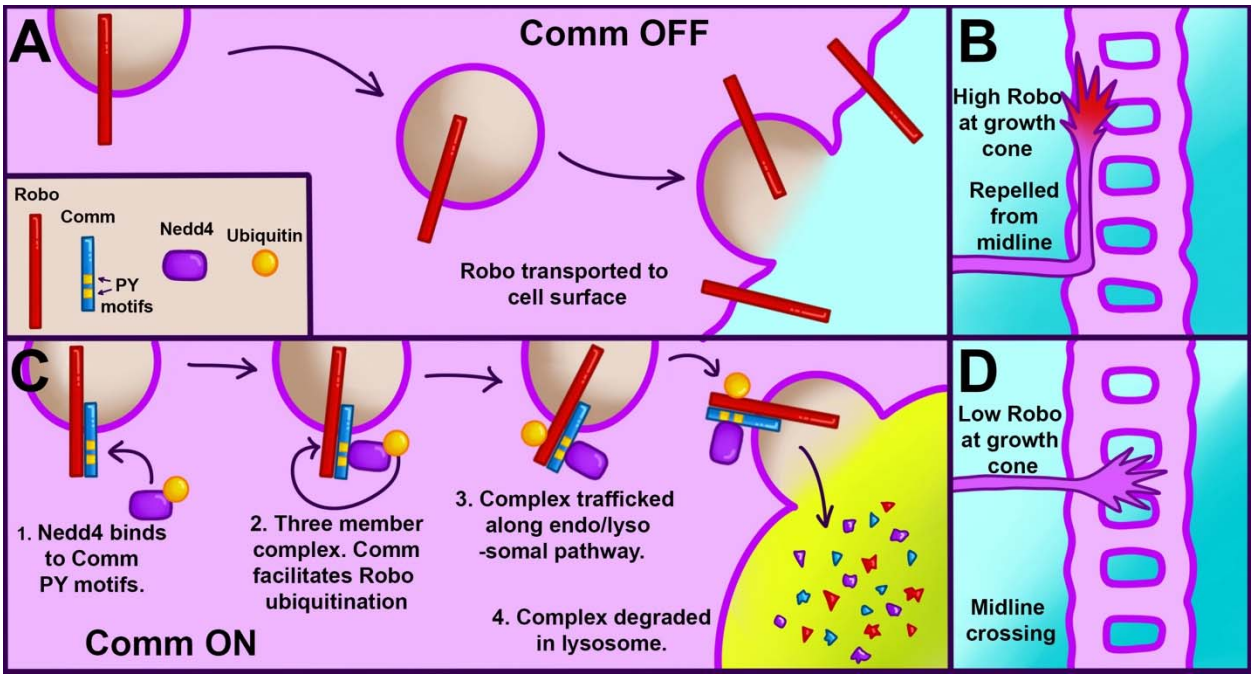

Figure 8: A schematic illustrating our proposed model for Robo1 downregulation in pre-crossing commissural axons. A-B) Localization and repulsive activity of Robo1 in neurons when Comm is absent. A) View of Robo1 trafficking down axons to the growth cone surface. In neurons not expressing Comm (such as ipsilateral or post-crossing neurons), Robo1 travels unimpeded to the growth cone surface. B). At the growth cone surface, Robo1 induces a repulsive response to slit, preventing midline crossing. C-D) Robo1 localization and repulsive activity in the presence of Comm. C) Comm facilitates Robo1 ubiquitination by recruiting Nedd4 via its PY motifs. Robo1 ubiquitination drives the entire Robo1/Nedd4/Comm complex to the lysosome. D) Due to lysosomal degradation, little Robo1 reaches the growth cone membrane. This lack of Robo1 renders axons insensitive to repulsion via slit, enabling them to cross the midline.

1166 **Supplementary figures and legends**

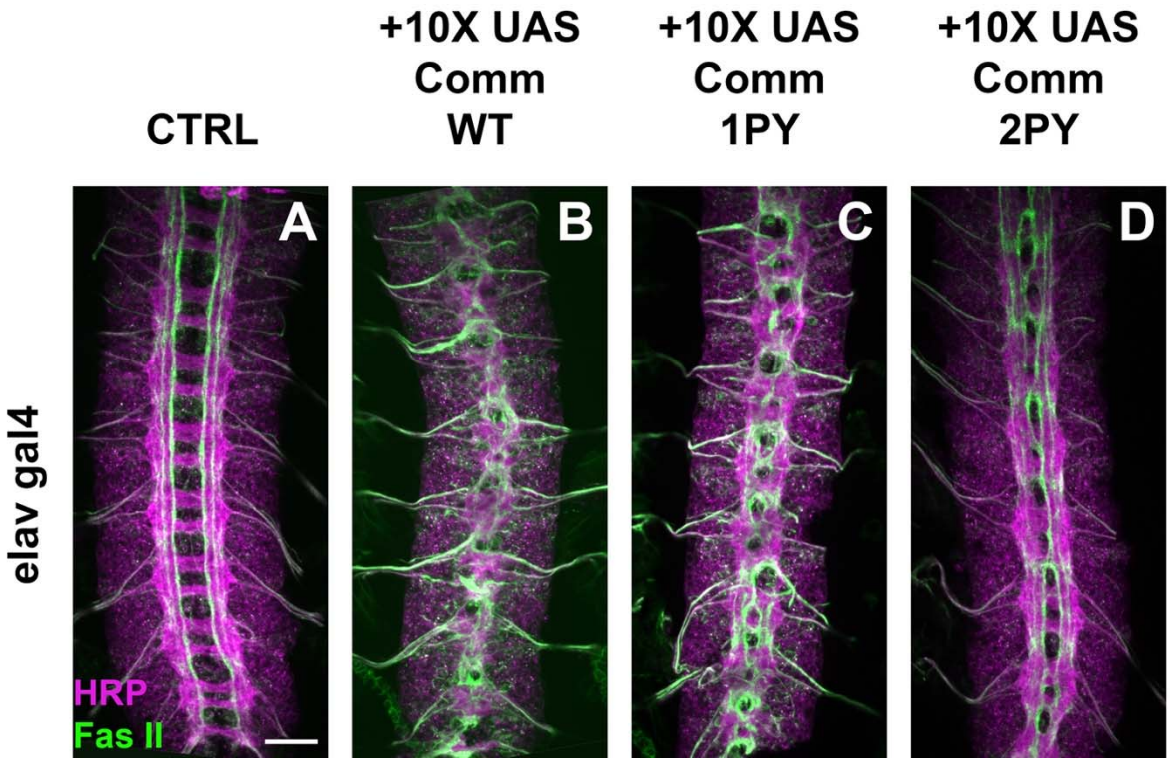

1167
1168 **Figure S1: Driving high levels of Comm, including those lacking functional PY motifs,**
1169 **induces ectopic midline crossing in ipsilateral neurons.** A-D) Nerve cords of embryos
1170 expressing no Comm (A), or 10X UAS transgenes for Comm WT(B) Comm 1PY (C) and Comm
1171 2PY (D). Embryos are stained with the pan neuronal marker HRP (green) and an antibody
1172 against FasII (magenta), which labels a population of ipsilateral neurons. Scale bar represents
1173 20μM.

1174

1175

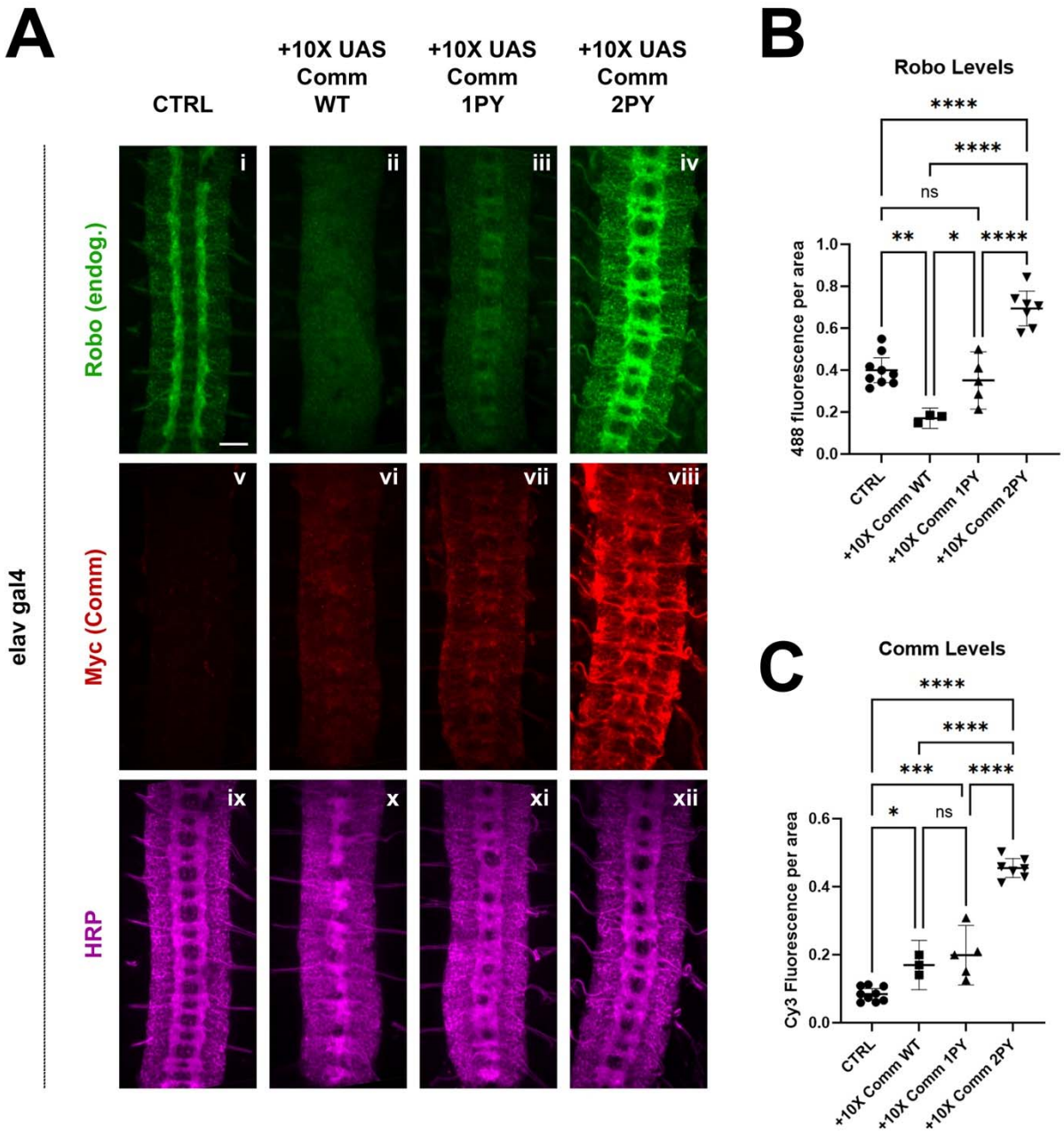

Figure S2: Robo expression in 10XUAS Comm transgenic flies. Stage 15-16 embryos expressing no Comm or 10X UAS Comm-myc variants under the pan neuronal elav gal4 driver. Embryos are stained for endogenous Robo1 (i-iv), Myc (v-viii), and pan-neuronal marker HRP (ix-xii). Scale bar represents 20μM. B) Quantification of endogenous Robo1 levels in stage 15-16 embryos expressing Comm variants under elav gal4 driver. Robo1 levels were measured by creating a mask of the axonal scaffold, measuring 488 fluorescence within the scaffold, and

1183 dividing by scaffold area. C) Quantification of Comm levels in stage 15-16 embryos expressing
1184 Comm variants under the *elavGal4* driver. Comm levels were measured by creating a mask of
1185 the whole nerve cord, measuring Cy3 fluorescence within the nerve cord, and dividing by nerve
1186 cord area. For B and C, groups were compared using ANOVA with Tukey's post-hoc test. **
1187 $p<0.01$ **** $p<0.0001$. Error bars represent 95% confidence intervals around the mean. Each
1188 data point represents one embryo.
1189
1190

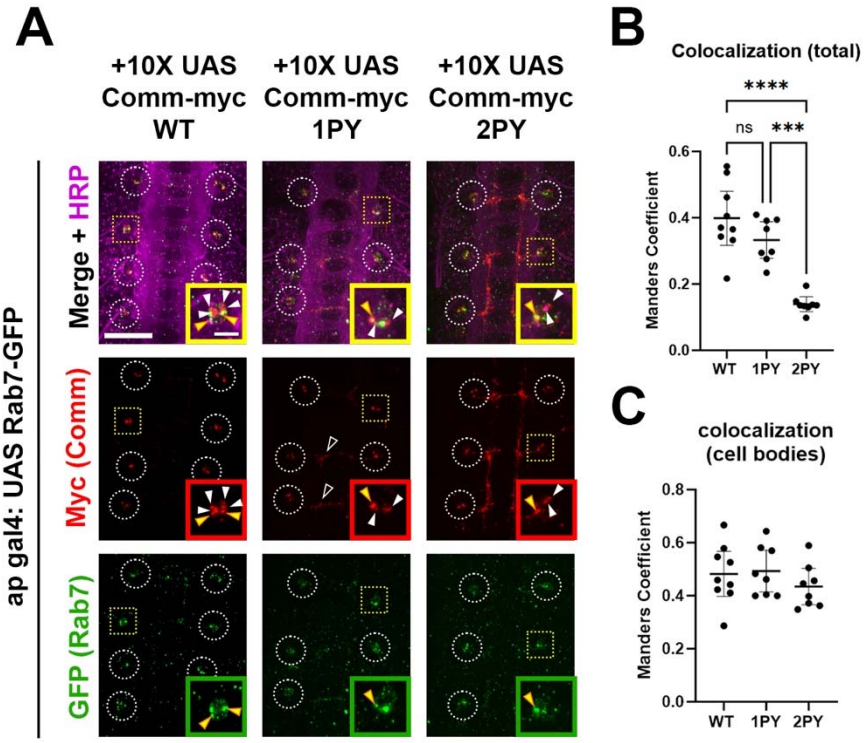

Figure S3: Colocalization of Comm with the late endosomal marker Rab 7. A) Stage 17 embryos expressing Rab7-GFP and WT or PY-mutant Comm myc variants under the *apGal4* driver. Embryos are stained with GFP (Rab7), Myc (Comm), and HRP (pan neuronal marker). Cell bodies are outlined with white circles except those that are enlarged in inset images, which are outlined with yellow squares. Within inset images, Comm/Rab7 co-positive puncta are indicated with yellow arrowheads and puncta containing Comm alone are indicated with white arrowheads. Scale bar represents 20μM. B) Total colocalization of Comm and Rab7. Proportion of areas of Comm expression that were also positive for Rab7 was calculated via pearson's coefficient within a mask created of the area of Comm expression using smoothened images from the Comm channel. C Colocalization of Comm and Rab7 within cell bodies. Proportion of areas of Comm expression that were also positive for Rab7 was calculated via pearson's coefficient within a mask created of cell bodies using smoothened images from the Lamp1 channel. For B and C, colocalization across conditions was compared via ANOVA (* $p<0.05$, **

1205 p<0.01). Error bars represent 95% confidence intervals around the mean. Each data point

1206 represents one embryo.

1207

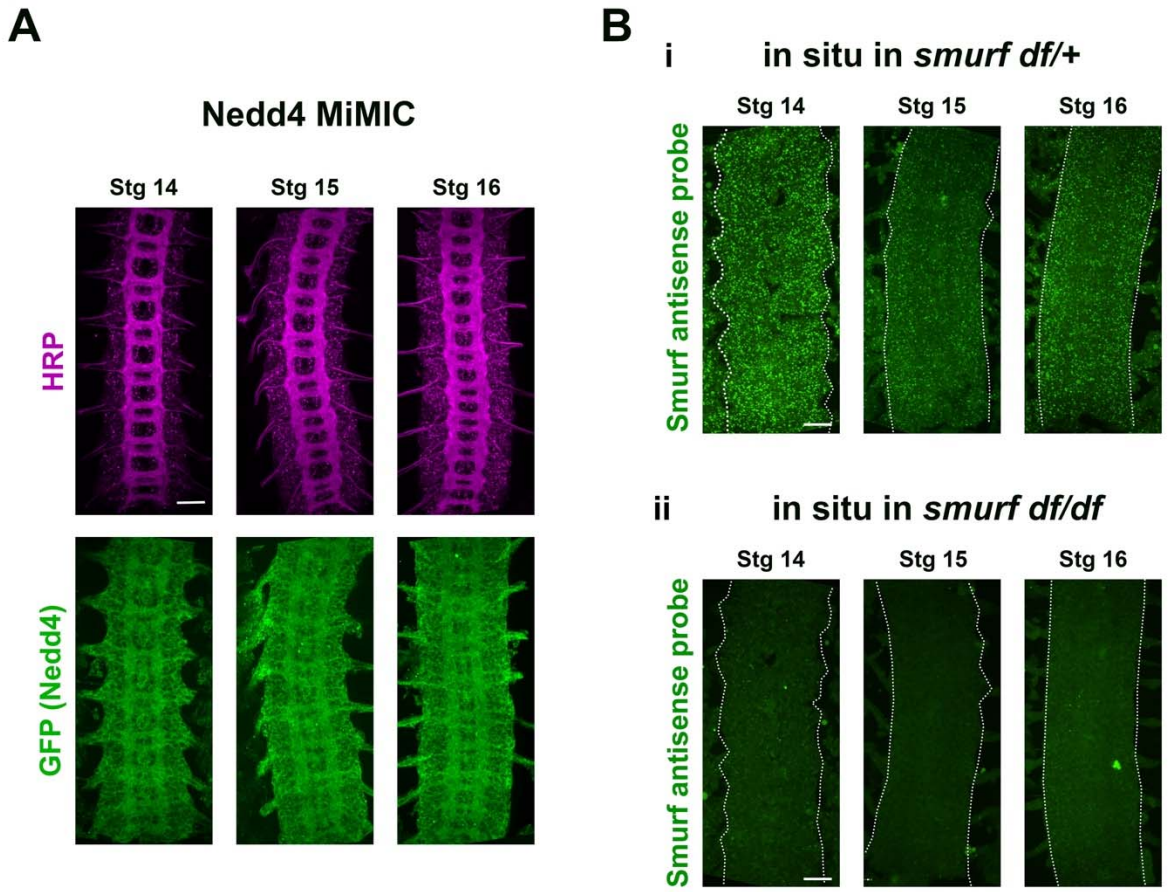

1208

1209 **Figure S4: Nedd4 and Smurf are expressed in the nerve cord at developmental stages**

1210 **when midline crossing occurs.** A. Nerve cords of Stage 14-16 Nedd4 MiMiC embryos, in

1211 which endogenous Nedd4 protein is tagged with GFP. Nedd4 expression was visualized using

1212 an antibody against GFP and the axon scaffold was visualized with HRP. B. In situ using an

1213 antisense probe against Smurf in Stage 14-16 embryos heterozygous (i) or homozygous (ii) for

1214 a chromosomal deletion covering the Smurf locus. Nerve cords are outlined with dotted lines. All

1215 scale bars represent 20μM.

1216

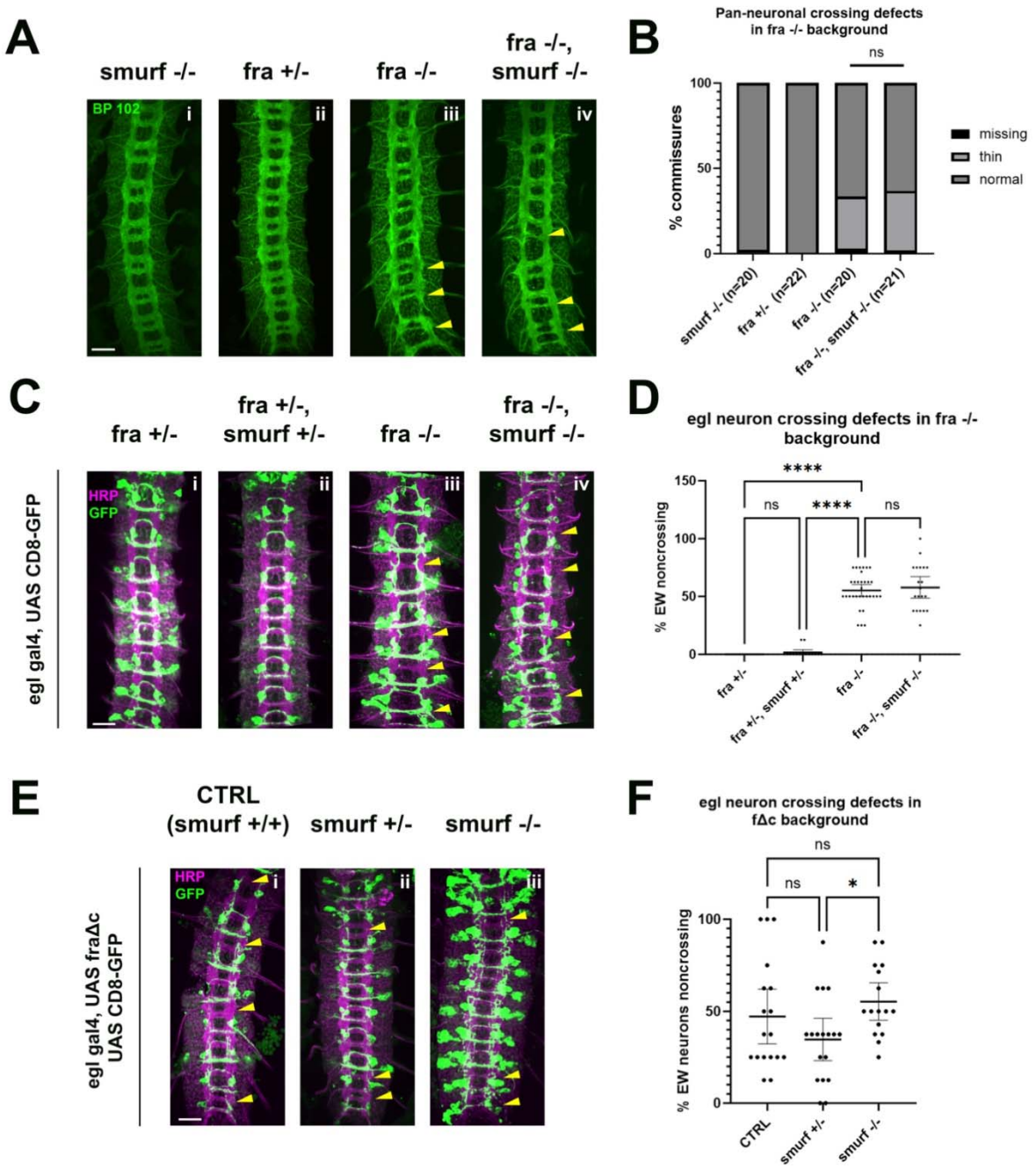

Figure S5: Smurf does not appear to be required for midline crossing *in vivo*. A-B) Loss of *smurf* does not enhance pan neuronal crossing defects in a *fra-/-* background. A) Stage 15-16 embryos with various combinations of *wild-type* and null *fra* and *smurf* alleles, stained with pan-neuronal marker BP102 (green). Commissures with crossing defects (either thin or completely missing) are indicated with yellow arrowheads. B) Quantification of crossing defects in embryos

1223 within the genotypes indicated in (A). Percentage of total crossing defects was compared across
1224 groups using ANOVA (** $p<0.01$, **** $p<0.0001$). N represents number of individual embryos. C-
1225 D) Loss of *smurf* fails to enhance EW crossing defects in a fra -/- background. C Stage 15/16
1226 embryos with various combinations of wt and null fra and nedd4 alleles, expressing GFP under
1227 the egl gal4 driver. Embryos are stained with pan-neuronal marker HRP, and GFP to visualize
1228 egl neurons. Commissures with EW crossing defects are indicated with arrowheads. D)
1229 Quantification of crossing defects in embryos within the genotypes indicated in C. Percentage of
1230 crossing defects was compared across groups using ANOVA (** $p<0.01$, **** $p<0.0001$). Each
1231 data point represents an individual embryo and error bars represent 95% confidence intervals
1232 around the mean. E-F) Loss of *smurf* fails to enhance EW crossing defects in the fraΔc
1233 background. E) Embryos with *smurf* mutations in fraΔc background. F) Quantification of EW
1234 crossing defects for the genotypes shown in E. Percentage of crossing defects was compared
1235 across groups using ANOVA (** $p<0.01$, **** $p<0.0001$). Each data point represents an
1236 individual embryo and error bars represent 95% confidence intervals around the mean. All scale
1237 bars represent 20μM.
1238

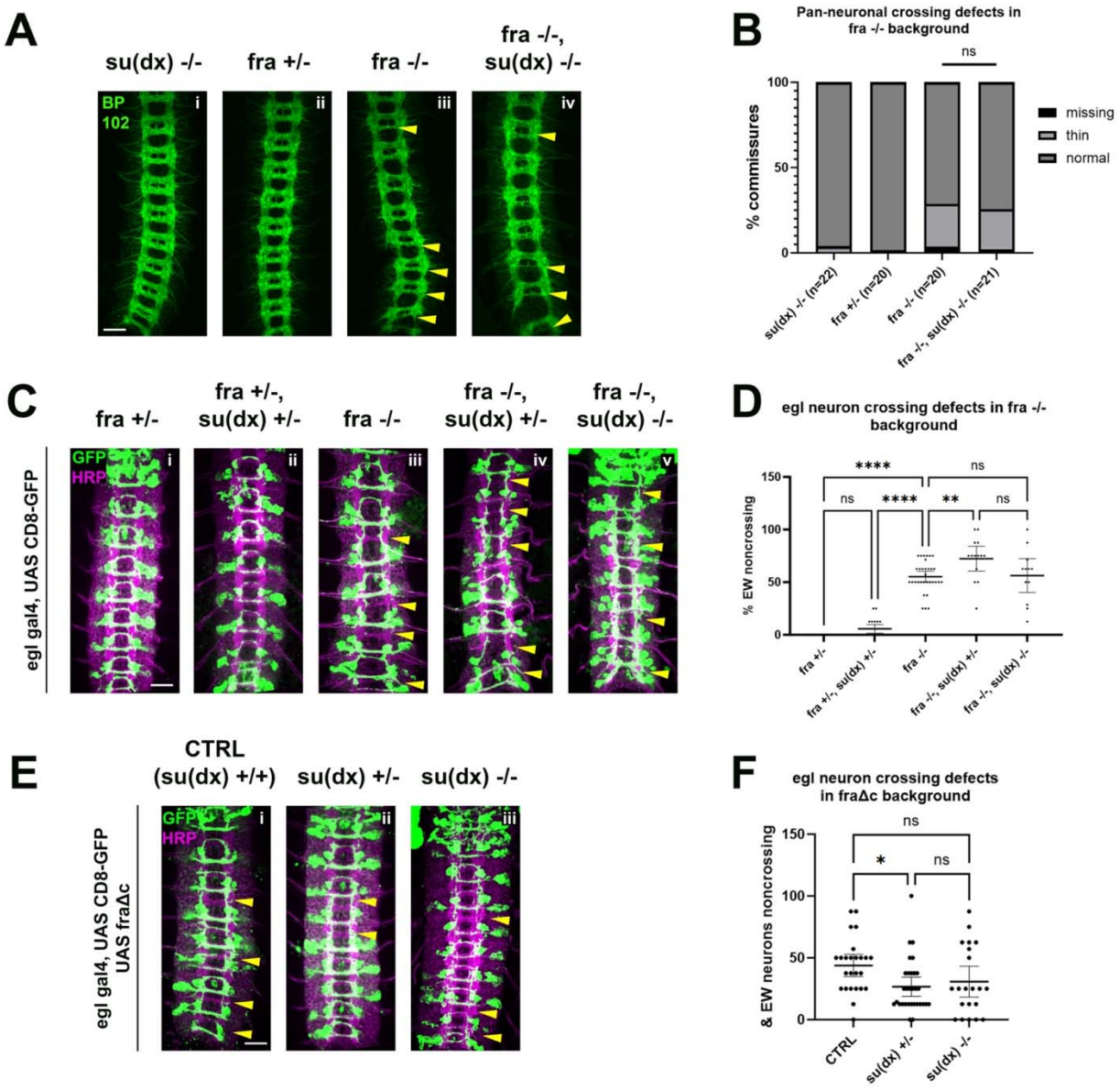

Figure S6: Su(dx) does not appear to be required for midline crossing *in vivo*. A-B) Loss of *Su(dx)* fails to enhance pan neuronal crossing defects in a fra-/- background. A) Stage 15/16 embryos with various combinations of *wild-type* and null *fra* and *Su(dx)* alleles, stained with pan-neuronal marker BP102 (green). Commissures with crossing defects (either thin or completely missing) are indicated with yellow arrowheads. B) Quantification of crossing defects in embryos within the genotypes indicated in A. Percentage of total crossing defects was compared across groups using ANOVA (** $p<0.01$, **** $p<0.0001$). N represents number of individual embryos. C-

1247 D) Loss of *Su(dx)* fails to enhance EW crossing defects in a *fra -/-* background. C Stage 15/16
1248 embryos with various combinations of *wild-type* and null *fra* and *nedd4* alleles, expressing GFP
1249 under the egl gal4 driver. Embryos are stained with pan-neuronal marker HRP, and GFP to
1250 visualize egl neurons. Commissures with EW crossing defects are indicated with arrowheads.
1251 D) Quantification of crossing defects in embryos within the genotypes indicated in C.
1252 Percentage of crossing defects was compared across groups using ANOVA (** $p<0.01$, ****
1253 $p<0.0001$). Each data point represents an individual embryo and error bars represent95%
1254 confidence intervals around the mean. E-F) Loss of *Su(dx)* fails to enhance EW crossing
1255 defects in the fraΔc background. E) Embryos with *Su(dx)* mutations in fraΔc background. F)
1256 Quantification of EW crossing defects for the genotypes shown in E. Percentage of crossing
1257 defects was compared across groups using ANOVA (** $p<0.01$, **** $p<0.0001$). Each data point
1258 represents an individual embryo and error bars represent95% confidence intervals around the
1259 mean. All scale bars represent 20μM**.**
1260
1261
1262
1263